RESEARCH TECHNICAL REPORT

Numerical Modeling of Sprinkler Activations and Spray Transport Under Sloped Ceilings

FM Global®

Numerical Modeling of Sprinkler Activations and Spray Transport Under Sloped Ceilings

Prepared by

Prateep Chatterjee and Karl V. Meredith

November 2015

FM Global
1151 Boston-Providence Turnpike
Norwood, MA 02062

PROJECT ID 0003055093

Disclaimer

The research presented in this report, including any findings and conclusions, is for informational purposes only. Any references to specific products, manufacturers, or contractors do not constitute a recommendation, evaluation or endorsement by Factory Mutual Insurance Company (FM Global) of such products, manufacturers or contractors. FM Global does not address life, safety or health issues. FM Global undertakes no duty to any party by providing this report or performing the activities on which it is based. FM Global makes no warranty, express or implied, with respect to any product or process referenced in this report. FM Global assumes no liability by or through the use of any information in this report.

Executive Summary

Working in partnership with the Fire Protection Research Foundation (FPRF), the research affiliate of the National Fire Protection Association (NFPA), this study investigates the impact of sloped ceilings on fire protection requirements and is aligned with the overall goal of the FPRF "Protection of Storage Under Sloped Ceilings – Phase 1" project. The goal of the FPRF project is to support the NFPA 13 Technical Committee in the development of new protection requirements to address sprinkler installation beneath sloped ceilings. Phase 1 of the project aims to develop a test plan for Phase 2 based on numerical modeling and a review of current storage configurations. Custom Spray Solutions, Inc. [i] has been contracted by FPRF to conduct the review of typical storage configurations and commodities that are stored under sloped ceilings. The numerical modeling work is performed by FM Global and is the focus of this report.

A numerical modeling study has been conducted to facilitate understanding of protection challenges associated with sloped ceilings. This study uses the computational fluid dynamics (CFD) code FireFOAM [ii, iii]. Validation simulations were first conducted to evaluate FireFOAM's capabilities of simulating flows below sloped ceilings. Predicted results for various ceiling inclinations showed good comparison with experimental data. Ceiling jets resulting from growing fires under sloped ceilings were then simulated to achieve the following:

- Evaluate sprinkler activation times and patterns from flow simulations under ceilings having a range of slopes, with large-scale growing fires as plume sources.
- Evaluate the effect of ceiling inclination on water mass flux distributions over a rack-storage commodity.
- Understand the effect of sprinkler orientation by performing spray simulations with sprinkler deflector parallel to the ceiling or to the floor.

The modeling work has been divided into two parts: 1) a sprinkler activation study, and 2) a sprinkler sprays investigation, as described below.

1. For sprinkler activation predictions, simulations have been performed of ceiling flows resulting from a growing fire on a 3-tier high rack storage array of FM Global Cartoned Unexpanded Plastic (CUP) commodity. The fire plume source had a maximum convective heat release rate (HRR) of 15 MW. Sprinkler sprays were not included in the activation calculations in order to isolate the activation patterns from suppression phenomena. Ceiling inclinations between 0° and 33.7° have been considered. Activation times and patterns below the inclined ceilings were compared against horizontal ceiling results. In addition to the ceiling clearance of 3.05 m (10 ft) considered

[i] Custom Spray Solutions, Inc., http://www.customspraysolutions.com

[ii] FireFOAM: available from http://www.fmglobal.com/modeling

[iii] Y. Wang, P. Chatterjee, and J. L. de Ris, "Large Eddy Simulation of Fire Plumes," *Proceedings of the Combustion Institute*, vol. 33, no. 2, pp. 2473-2480, 2011.

in the study, the effect of increasing the ceiling clearance to 6.1 m (20 ft) was also investigated. Comparison was also made between quick-response, ordinary temperature (QR/OT) and standard-response, high temperature (SR/HT) sprinklers.

2. The effect of ceiling slope and deflector orientation on sprinkler spray were investigated. A K200 lpm/bar$^{0.5}$ (K14.0 gpm/psi$^{0.5}$) pendent sprinkler has been selected in the simulations as its injection properties are well characterized by measurements [iv] and available as model inputs. Sprinkler spray simulations were conducted by selecting fixed fire source sizes for two scenarios: 1) when one sprinkler above the ignition location activates, and 2) when four sprinklers operate. Water mass flux distributions on top of the rack storage array were compared for various ceiling inclinations and sprinkler deflector orientations.

Based on the range of conditions explored in the present study, the following conclusions can be drawn:

- Results from activation simulations involving QR/OT sprinklers show that ceilings up to and including 18.4° inclination have similar activation times and patterns as horizontal ceiling for the four sprinklers immediately adjacent to the fire source.
- Increasing the inclination to 26.6° produces significant delays in activations on the lower side of the ceiling. The number of sprinklers activated on the elevated side also greatly exceeds the number of activations on the lower side when the ceiling inclination is ≥26.6°.
- For SR/HT sprinklers, the average delay time for activations of the four sprinklers surrounding the ignition location increases for the 18.4° inclination case. Four more activations take place in the elevated section before the sprinklers below the lower side activate, indicating the activation pattern skewness is accentuated with the use of these sprinklers. It is also to be noted that, compared to the QR/OT sprinklers, these sprinklers provide greater activation delays on average.
- Based on the two clearances included in the activation simulations for the 18.4° inclined ceiling (3.05 m and 6.1 m or 10 ft and 20 ft), it was found that increasing the ceiling clearance to 6.1 m (20 ft), the average activation time for the four sprinklers surrounding the ignition location increased by ~3 s and ~5 s for QR/OT and SR/HT sprinklers, respectively. Such activation time delays may have an adverse impact on protection design.
- For spray calculations involving a single sprinkler located directly above the ignition location, it was found that the deflector orientation strongly affects the water flux that reaches the fire source and the pre-wetting region. As the ceiling inclination increases, the water flux on top of the commodity was found to reduce when the sprinkler deflector was kept parallel to the ceiling. This reduction of water flux was significantly greater when a 600 kW fire plume was present (25% for the 18.4° and 49% for the 33.7° ceilings). On the other hand, as the inclination was increased, the parallel-to-the-floor orientation could maintain a fairly constant water flux to the fire region.
- For a fire plume located among four sprinklers (henceforth known as “among four sprinklers” configuration), it was determined that the ceiling slope at 33.7° adversely impacts the spray

[iv] X. Zhou, S. P. D’Aniello, and H.-Z. Yu, "Spray Characterization Measurements of a Pendent Fire Sprinkler," *Fire Safety Journal*, vol. 54, pp. 36-48, 2012.

density on the fire because of a highly skewed activation pattern, which results in the first four sprinkler activations occurring below the elevated side of the ceiling. For the 33.7° case, the water flux to the fire region is reduced by 54-76% as compared to the horizontal ceiling case.

- For ceiling slopes 18.4° and below, results are less sensitive to sprinkler orientation for the fire plume among four sprinklers case than for the case of a single sprinkler centered over the fire plume. This is because the activations downward from the centerline for the parallel-to-ceiling case actually result in water being projected towards the fire region. This observation is based on the assumption that four sprinklers surrounding the fire source activate simultaneously, and only the water flux on top of the fire source (3.05 m x 3.05 m [10 ft x 10 ft] area) are evaluated.
- Considering the significant effect of the deflector orientation on the water flux for a sprinkler above the ignition location and the relatively reduced effect of the orientation for the among four sprinklers case, the orientation parallel to the floor is preferable for a variety of fire scenarios among the cases studied.

Further evaluations of the conclusions should be made by conducting large-scale fire tests and/or by conducting numerical simulations. Several aspects have been neglected while conducting this study as the goal was to capture the first order physical effects on sprinkler activations and spray patterns. Some of these aspects are the presence of end-walls in buildings, obstructions to the ceiling flows caused by purlins and girders, inclusion of suppression phenomena in the modeling, etc. Before making general recommendations towards sprinkler protection schemes, it would be prudent to consider the effects of these aspects.

Abstract

In the present study, a numerical model based investigation has been conducted to facilitate understanding of protection challenges associated with sloped ceilings. The modeling study has been conducted using the computational fluid dynamics (CFD) code FireFOAM. First, a validation study for flows under ceilings of varying slopes has been presented. Second, ceiling jets resulting from growing fires on a 3-tier high CUP rack-storage commodity have been simulated to investigate the effect of ceiling slope on sprinkler activations. For quick-response, ordinary temperature sprinklers, simulation results show that for the fire source being evaluated, ceilings up to and including 18.4° inclination have similar activation times and patterns as horizontal ceiling for the four sprinklers immediately adjacent to the fire source. Finally, spray transport simulations have been conducted to evaluate the effect of ceiling slope and sprinkler installation orientations on water flux distributions. Results indicated that the sprinkler deflector parallel to the floor is a preferable orientation.

Acknowledgements

The authors would like to offer their sincere gratitude to Dr. Ankur Gupta for making available the newly developed FireFOAM CUP fire growth model and for his assistance in the implementation of the pyrolysis mapping boundary condition. Dr. Yi Wang has provided key technical feedback on several occasions and his contributions towards the completion of the project are well appreciated. Technical feedback, from the time of proposal development to the completion of the project, was provided by several people. Key among them are Messrs. Weston Baker, David Fuller and Benjamin Ditch and Drs. Christopher Wieczorek, Francesco Tamanini and Sergey Dorofeev. Dr. Louis Gritzo is acknowledged for his continued support towards the successful completion of the project. The NFPA FPRF technical panel members, the Custom Spray Solutions, Inc. team and Ms. Amanda Kimball of FPRF are thanked for providing their feedback.

Table of Contents

List of Figures

List of Tables

1. **Introduction**

Working in partnership with the Fire Protection Research Foundation (FPRF), the research affiliate of the National Fire Protection Association (NFPA), this study investigates the impact of sloped ceilings on fire protection requirements and is aligned with the overall goal of the FPRF "Protection of Storage Under Sloped Ceilings – Phase 1" project. The goal of the FPRF project is to support the NFPA 13 Technical Committee in the development of new protection requirements to address sprinkler installation beneath sloped ceilings. Phase 1 of the project aims to develop a test plan for Phase 2 based on numerical modeling and a review of current storage configurations. Custom Spray Solutions, Inc. [1] has been contracted by FPRF to conduct the review of typical storage configurations and commodities that are stored under sloped ceilings. The numerical modeling work was performed by FM Global and is the focus of this report.

In the present study, a numerical model based investigation has been conducted to facilitate understanding of protection challenges associated with sloped ceilings. The modeling study has been conducted using the computational fluid dynamics (CFD) code FireFOAM [2] [3]. Ceiling jets resulting from growing fires below sloped ceilings have been simulated to investigate the effect of ceiling slope on sprinkler activations. Spray transport simulations have also been conducted to evaluate the effect of sprinkler installation orientations.

1.1 Literature Survey

Several concerns for storage under sloped ceilings have been recently voiced [4]. The major concerns are 1) possible delays in sprinkler activations due to the biased, upward flow of hot gases under the sloped ceilings, and 2) sprinklers further away from the fire source activating first (with delayed activation times), causing the need for higher sprinkler densities resulting from larger fire size [4].

Large-scale suppression testing results with sloped ceilings are not readily available in literature for sprinkler protection design [4]. Few small- and intermediate-scale tests have been conducted in the past to investigate sloped ceilings. Vettori [5] investigated residential sprinkler activations in compartment fire scenarios involving ceiling inclinations of 0°, 13° and 24°. Kung et al. [6] conducted small-scale tests with pool fires measuring ceiling jet velocities and temperatures for ceiling heights of 0.28 m (0.92 ft) – 0.89 m (2.92 ft) and ceiling inclinations of 10°, 20° and 30°. Floyd et al. [7] reported intermediate-scale test data on performance of residential sprinklers with ceiling heights of 2.7 m (8.9 ft) – 5.7 m (18.7 ft) and inclinations of 18.4° and 33.7°. Bill and Hill have also reported residential sprinkler response in manufactured homes with a ceiling height of 2.1 m (6.9 ft) and inclination of 10° [8]. The majority of the above mentioned studies involved use of residential sprinklers and compartment or tunnel fire scenarios, generally with weak plume sources.

Due to the excessive cost of large-scale testing, numerical modeling becomes an attractive tool for investigation of sloped ceiling flows, provided the models are used within their limitations. Few numerical modeling studies have been conducted in the past with respect to sloped ceilings. Davis et al. [9] simulated sprinkler response under sloped ceilings using the FLOW3D software and reported smoke detector and

thermal sensor optimum locations for two fire sizes (100 kW and 1 MW). Vettori [5] applied an earlier version of the Fire Dynamics Simulator (FDS) [10] to predict sprinkler activation times for growing fires under sloped ceilings with a maximum heat release rate (HRR) of 1.1 MW. The simulated activation times were found to be in general agreement with the observed activation times. Floyd et al. [11] modeled flows under sloped ceilings using FDS, evaluating smoke detector spacing requirements.

In a later study, Floyd et al. [7] applied FDS modeling with a 300 kW fire and compared predicted ceiling jet temperatures with test results. In addition, water distribution patterns at the floor level were also predicted and compared with measurements [7]. In the study, residential sprinklers were placed with the deflectors parallel to the sloped ceilings. In a recent study, Carlsson [12] has used FDS modeling to predict sprinkler activations under sloped ceilings, concluding that sprinkler protection can be feasible for inclinations >9.5°, but with limitations, e.g., the use of low RTI, ordinary temperature sprinklers. The study also highlights the issues involved with modeling the sloped ceilings using a "saw-tooth" mesh (see FDS validation guide [10] for details). Methods of mitigating the issue of vorticity generation at the sharp corners of the ceiling mesh resulting in adverse effects on the flow predictions were discussed; however, the "saw-tooth" mesh was retained for the sprinkler activation predictions by Carlsson [12].

Based on previous testing, FM Global currently accepts storage sprinklers installed under ceiling inclinations ≤10° and when in-rack sprinkler protection is not provided [13] [14]. When the ceiling inclination exceeds 10°, installation of a flat, continuous false ceiling is recommended [14]. For inclinations ≤10°, rack storage protection is based on the presence of excessive clearance as outlined in FM Global Property Loss Prevention Data Sheet 8-9, Storage of Class 1, 2, 3, 4 and Plastic Commodities [13]. Similar to the FM Global recommendations, NFPA 13 recommends the use of false/drop ceilings in case the ceiling inclinations exceed 9.5° [15]. Another option recommended by NFPA 13 is the use of a dynamic analysis to determine protection requirements on a case-by-case basis.

Differences in recommendations on sprinkler orientations exist between FM Global and NFPA 13: according to FM Global Property Loss Prevention Data Sheet 2-0, Installation Guidelines for Automatic Sprinklers [14], sprinkler deflector orientation is to be parallel to the floor, whereas NFPA 13 recommends deflector orientation parallel to the ceiling slope [15]. Sprinkler orientation can affect spray distribution over the underlying protected commodity.

1.2 Objectives

Although the numerical studies mentioned above have explored physical aspects of the sloped ceiling problem, several issues remain unaddressed. Key among the issues are the application of large-scale growing fires in the simulations and effectiveness of water sprays in controlling fire growth when the sprinkler deflector orientation is either parallel to the sloped ceiling or to the floor. Custom Spray Solutions, Inc. worked to address the latter issue of sprinkler orientation in a recent study [16]. The study, however, did not involve the presence of fire plumes.

The present numerical study is undertaken to bridge the knowledge gaps in understanding the challenges of sprinkler protection under sloped ceilings. The aim of the study is to provide guidance to Phase 2 of the FPRF project by conducting the following:

- Evaluate sprinkler activation times and patterns from ceiling jet simulations under ceilings having a range of slopes, with large-scale growing fires as plume sources.
- Evaluate the effect of ceiling inclination on water mass flux distributions over a rack-storage commodity.
- Understand the effect of sprinkler orientation by performing spray simulations with two sprinkler orientations–deflector parallel to the ceiling or to the floor.

1.3 Technical Approach

The modeling work has been divided into two parts: 1) a sprinkler activation study, and 2) a sprinkler sprays investigation, as described below.

1. For sprinkler activation predictions, simulations have been performed of ceiling flows resulting from a growing fire on a 3-tier high rack storage array of FM Global Cartoned Unexpanded Plastic (CUP) commodity. Ceiling clearances of 3.05 m (10 ft) and 6.1 m (20 ft) were selected and ceiling inclinations between 0° and 33.7° have been considered. The ranges for ceiling clearance and inclination have been selected based on prevailing storage conditions in the industry. A summary of the parameters used in the sprinkler activation study is included in Table 1-1 below.

Table 1-1: Parameters for the sprinkler activations simulations

Fire plume source	3-tier high rack storage of CUP commodity (growing fire HRR)					
Ceiling clearances (H)	3.05 m (10 ft)					6.1 m (20 ft)
Ceiling inclinations (θ)	0°	9.5°	18.4°	26.6°	33.7°	18.4°
Ceiling slopes	0	0.167 2 / 12 in.	0.333 4 / 12 in.	0.5 6 / 12 in.	0.667 8 / 12 in.	0.333 4 / 12 in.

2. The effect of slope and deflector orientation on sprinkler spray were investigated. A K200 lpm/bar$^{0.5}$ (K14.0 gpm/psi$^{0.5}$) pendent sprinkler has been selected as its injection properties are well characterized by measurements [17]. The water flux distribution on top of the rack storage array has been recorded. The water flux estimations have been made for the ignition location under one sprinkler as well as when the ignition location is between four sprinklers. A summary of the parameters used in the sprinkler sprays study is included in Table 1-2.

Table 1-2: Parameters for sprinkler sprays simulations

Fire plume source		3-tier high rack storage of CUP commodity (fixed HRR)		
Ceiling clearances (H)		3.05 m (10 ft)		
Ceiling	**inclinations (θ)**	0°	18.4°	33.7°
	slopes	0	0.333	0.667
Sprinkler type		K200 lpm/bar$^{0.5}$ (K14.0 gpm/psi$^{0.5}$) at 3.4 bar (50 psi)		
Deflector orientations		Parallel to ceiling		Parallel to floor

Figure 1-1 below shows the computational setup with unconfined ceilings at different inclinations above a 3-tier high rack storage arrangement of CUP commodity. Open boundary conditions were simulated on all sides. The unconfined ceiling configurations shown in the figure correspond to scenarios of the fire source being located far away from side walls, which tend to cause recirculation of the product gases and can lead to earlier activations. Because of this choice, the configurations selected for investigation represent worst case scenarios for sprinkler activations.

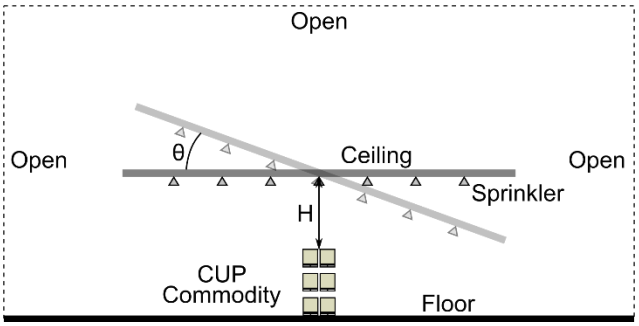

Figure 1-1: Computational setup (not to scale) showing the 3-tier high rack storage arrangement located H height below unconfined ceilings (horizontal and inclined at θ angles).

2. **Numerical Model**

2.1 FireFOAM Solver

The FireFOAM code [2], which is based on the open source framework OpenFOAM [18], is used in the current study. OpenFOAM supports unstructured meshes with cells of arbitrary shapes permitting flexibility in ceiling jet mesh generation [19]. The "saw-tooth" mesh used in previous studies [5] [7] [12] has been avoided in the current set of simulations.

Models for large eddy simulations (LES) of buoyant turbulent diffusion combustion [3], thermal radiation heat transfer from soot emission [20] [21], and solid-phase pyrolysis [22] [23] are included in FireFOAM for fire growth simulations. Wall bounded fires have been accurately simulated with the application of a convective heat flux model [24]. Ceiling flows have also been simulated and temperature and velocity predictions in the ceiling jet have been close to experimental data [25].

Multiphase flow aspects of fire suppression are also included in FireFOAM. A Lagrangian transport model is employed to simulate water droplets originating from a sprinkler, transporting through fire plumes, and impinging on burnt and/or unburnt surfaces. A thin film model is included and validated for simulating the flow and interaction of liquid water with solid fuel surfaces [26] [27]. A response time index (RTI) model has been included in FireFOAM and has been verified to give accurate estimates of sprinkler activation [28]. Actual delivered density (ADD) predictions have been made by the model [29] and suppression of rack storage commodity has successfully been simulated [28] [30].

In the present study, the combustion, turbulent flow and radiation models are used to simulate the fire plumes and the resulting ceiling jets, and the Lagrangian model is used for sprinkler spray transport. The pyrolysis model is also applied to generate the spatiotemporally varying fuel mass loss rates from a Cartoned Unexpanded Plastic (CUP) commodity. It should be noted that in the current study, suppression simulations have not been conducted. FireFOAM version 2.2.x [2] has been used for the simulations.

2.1.1 Sloped Ceiling Flow Validation

A validation exercise was undertaken to evaluate the FireFOAM's capabilities of predicting ceiling jets under sloped ceilings. The experimental configuration from Kung et al. [6] was selected for the simulations. The mid-point of a 2.44 m x 2.44 m (8 ft x 8 ft) ceiling was selected to be 0.89 m (2.9 ft) above a 22.8 cm (9 in.) diameter burner, as shown in Figure 2-1(a). Heptane was selected as the fuel source, producing a fire with an average chemical heat release rate (HRR) of 20 kW. A constant overall radiant fraction of 35% was applied in the simulations resulting in a convective HRR of 13 kW. Four cases were simulated with ceiling inclinations at 0°, 10°, 20° and 30°. A mesh resolution of approximately $(6.5\ \text{mm})^3$ was used in the plume and ceiling jet regions (see Figure 2-1(b) for mesh details). The selected resolution was determined from a mesh independence study. Results from the simulations were time-averaged for a duration of 120 s. Results are reported for the non-dimensional temperature rise, $\Delta T/\Delta T_c$, and velocity in the direction of the ceiling slope, v_θ/w_c, 1.3 cm (0.5 in.) perpendicular distance below the ceiling. Here, ΔT is the temperature rise from the ambient ($T - T_\infty$), ΔT_c is the plume centerline temperature rise ($T_c - T_\infty$),

v_θ is the velocity parallel to the ceiling slope, and w_c is the centerline vertical velocity of the plume. ΔT_c and w_c are computed values from a plume simulation where the ceiling was excluded. In Figure 2-2 time-averaged temperature contours are shown when the ceiling is inclined at 30° to the horizontal. The ceiling jet thickness under the elevated side of the ceiling is larger than that under the lower side. Flow reversal can be observed below the lower side, where the temperature becomes the same as the ambient.

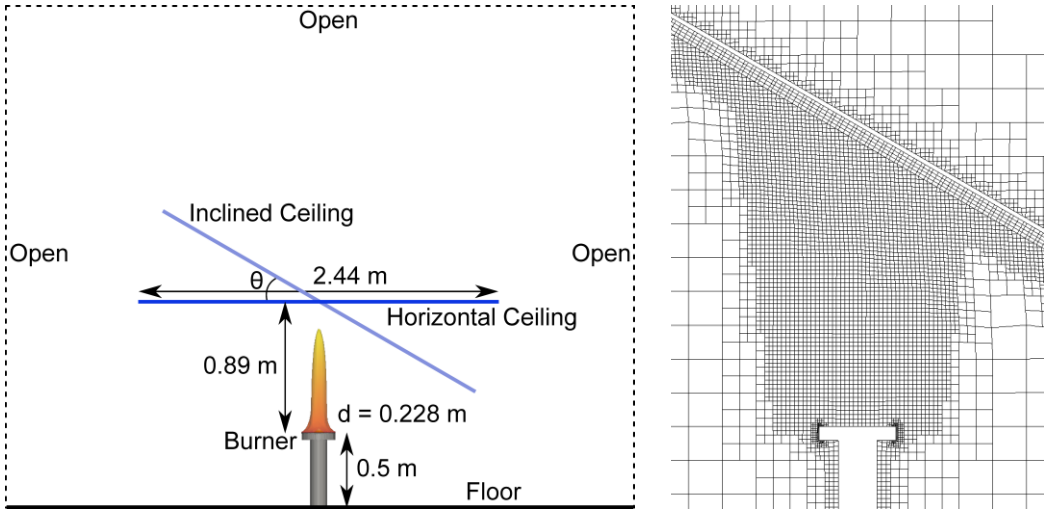

Figure 2-1: Computational setup used in the validation study showing (a) a horizontal and an inclined ceiling at θ angle located 0.89 m above a 0.228 m diameter burner (elevated by 0.5 m), and (b) a close-up image of the mesh for a 30° inclined ceiling.

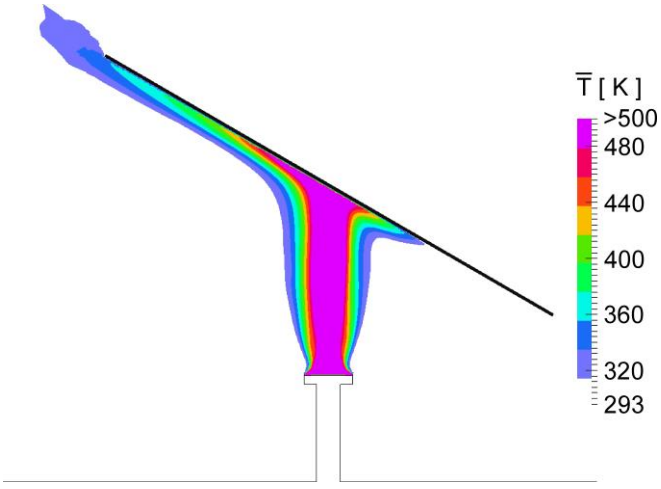

Figure 2-2: Time-averaged temperature contours below a ceiling inclined at 30° to the horizontal. Flow resulting from a weak plume is generated by a 13 kW convective HRR heptane fire. Temperature contours above 500 K are not included.

In Figure 2-3 the predicted results are compared with the entire experimental dataset (all inclination angles). Comparison of the non-dimensional temperature rise ($\Delta T/\Delta T_c$), shown in Figure 2-3(a), are reasonable for a significant portion of the temperature range. Larger differences between predictions and experimental temperature rise can be observed for $\Delta T/\Delta T_c > 0.8$. In the case of non-dimensional velocity (v_θ/w_c), comparisons for $v_\theta/w_c > 0.4$ fall within the experimental uncertainty. For $v_\theta/w_c < 0$, comparisons are generally good except for some locations. It must be mentioned here that the velocity measurements were made at 3.8 cm (1.5 in.) perpendicular distance below the ceiling using bi-directional probes which were aligned with the ceiling slope [6]. The velocity data was then extrapolated to values at 1.3 cm (0.5 in.) below the ceilings assuming half of a Gaussian velocity profile distribution and reported in Ref. [6]. This extrapolation technique (assuming half of a Gaussian profile) is not valid for locations below the lower side of the inclined ceilings where flow reversal takes place. The differences in predicted and experimental values for $v_\theta/w_c < 0$ can, therefore, be attributed to errors in the extrapolation method.

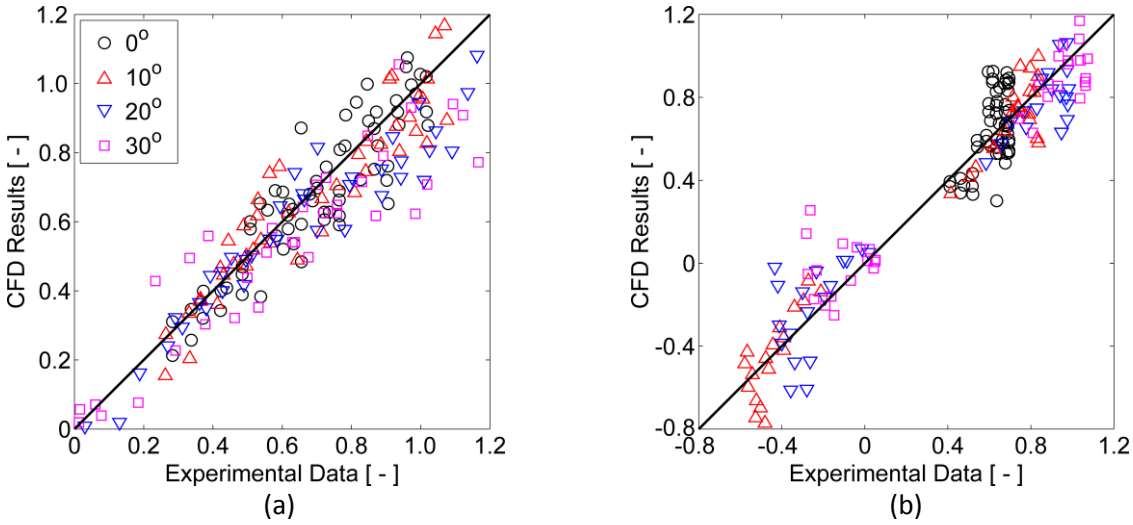

Figure 2-3: Comparison of predicted values with experimental data [6] for non-dimensional (a) temperature rise, and (b) velocity for all ceiling inclination cases. Negative velocities are present below the lower side of the inclined ceilings. Data points (symbols) lying on the black line represent perfect matches between predicted and experimental data. For the 0° case, experimental data are only reported on one side of the ceiling.

Detailed comparisons between predicted and experimental data are shown in Figure 2-4. Data are plotted against non-dimensional radial distance, r/b_c, where b_c is the plume half-width (computed from the plume simulation and defined as the radial distance where $\Delta T/\Delta T_c = 0.5$). Positive r/b_c locations are below the elevated side of the ceilings and negative locations below the lower side. Positive velocities on the lower side indicate flow reversal. However, following the experimental study [6], the location where temperature rise is approximately zero is considered as the penetration distance (i.e., where flow reversal occurs).

For the 0° inclination case, the predicted non-dimensional temperature rise shows very good comparison with the experimental data distribution as can be observed in Figure 2-4(a). The corresponding predicted

non-dimensional velocity, also compared in Figure 2-4(a), shows general agreement with the experimental data. When the ceiling inclination is 10°, predicted temperature and velocity show good agreement with experimental data, except at few locations below the lower side of the ceiling, as seen in Figure 2-4(b).

Increasing the ceiling inclination to 20° and 30°, we observe in Figure 2-4(c) and (d) that the predicted temperature slopes on the elevated side follow the experimental data distribution, with some over-prediction for the 30° case. The penetration distance for both inclinations, though, are accurately predicted. Velocity predictions on the elevated side show reasonable agreement with experimental data; however, some differences are present on the lower side. As described above, the experimental uncertainties on the lower side are large due to the extrapolation technique used in the experiments. This is more evident in Figure 2-4(d), where experimental velocities on the lower side immediately adjacent to the mid-point are positive, indicating the presence of flow reversal. However, this is inconsistent with the temperature profile in Figure 2-4(d) which shows $r/b_c = -4.9$ as the penetration distance. On the other hand, the simulation results shown in Figure 2-4(d) demonstrate consistent predictions of penetration distance in both velocity and temperature profiles. The comparison of the predicted temperatures and velocities with experimental data shows that FireFOAM accurately models flows below sloped ceilings. Key features, like the penetration distance are accurately predicted (see Table 2-1). It should be mentioned here that the penetration distance for the 10° ceiling was extrapolated from the experimental data and predicted temperature rise.

The validated model is next applied for large-scale simulations involving strong plume driven ceiling jets. The computational setup, fire growth modeling in the CUP rack storage array, boundary conditions applied and the sprinkler activation and spray setups are sequentially described below.

Table 2-1: Non-dimensional penetration distances for the inclined ceilings.

Ceiling inclination (°)	Non-dimensional penetration distance	
	Exp Data [6]	CFD Prediction
10	9.80*	10.75*
20	6.15	6.88
30	4.97	4.79

*extrapolated values

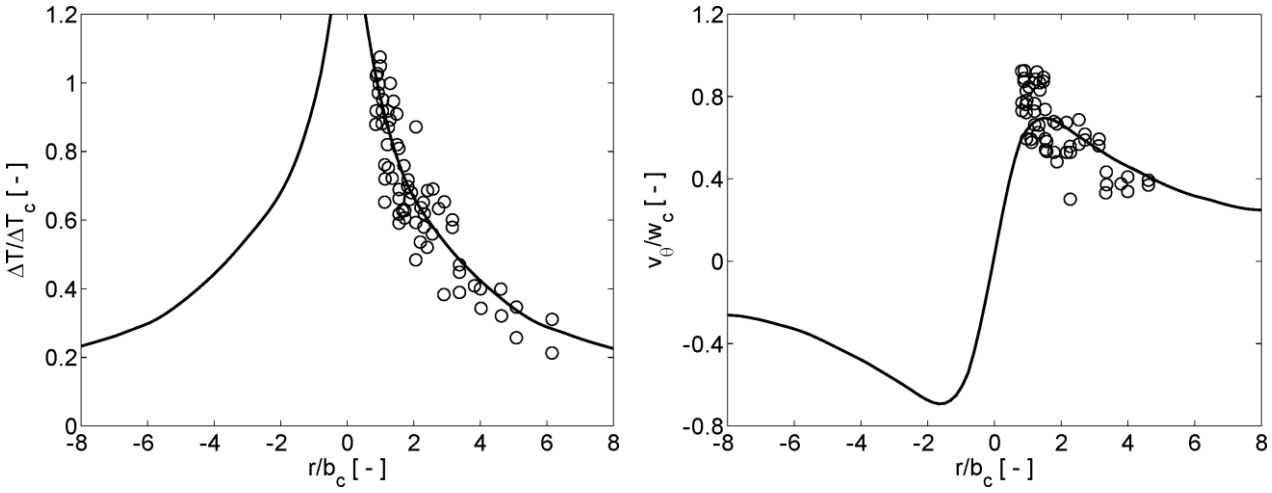

(a) 0°

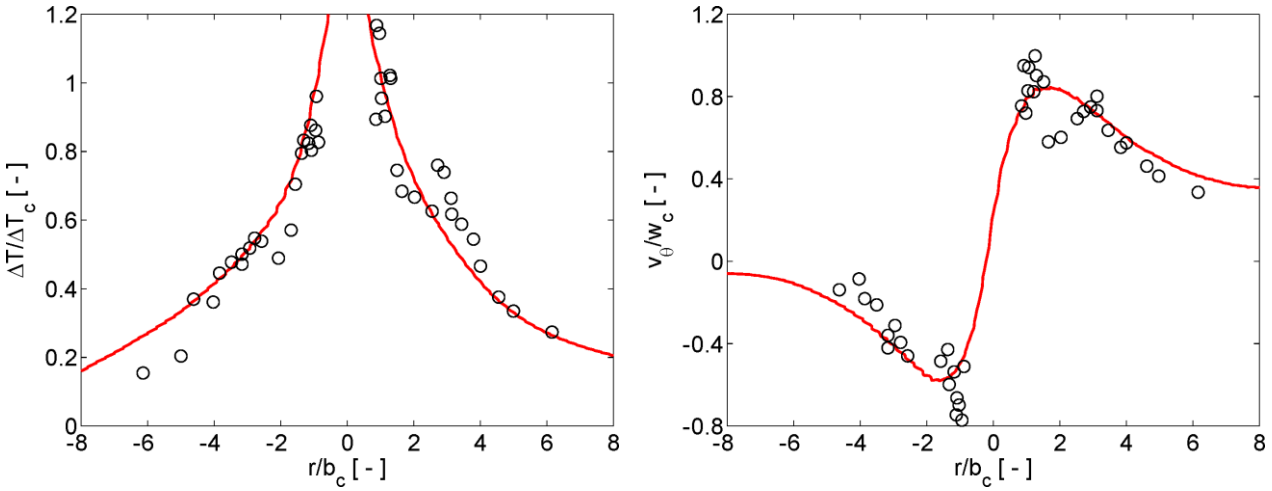

(b) 10°

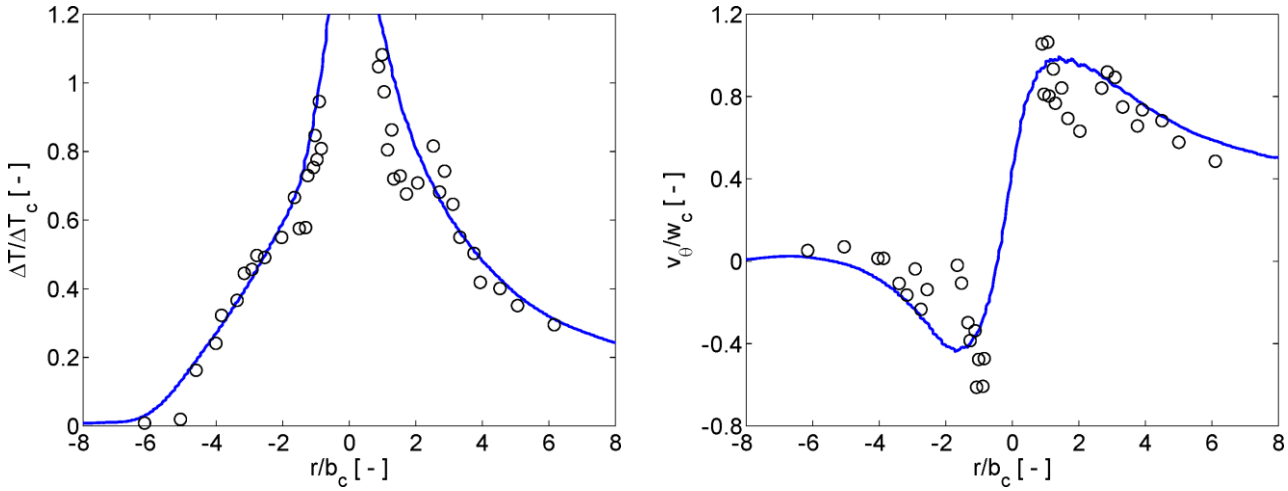

(c) 20°

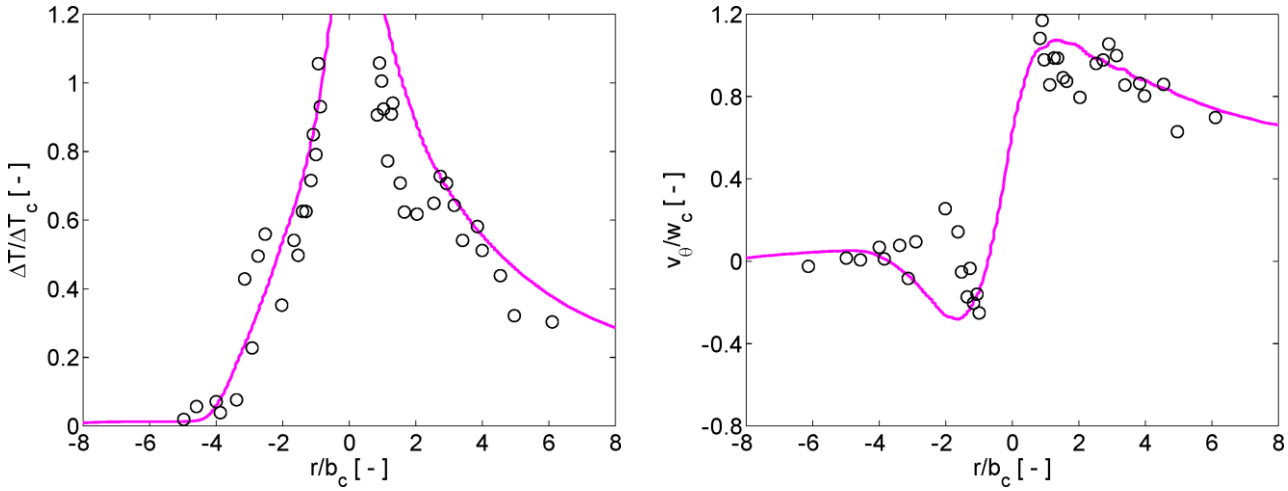

(d) 30°

Figure 2-4: Comparison of non-dimensional temperature rise and velocity between experimental data (symbols) [6] and predictions (curves) for four ceiling inclinations: (a) 0°, (b) 10°, (c) 20°, and (d) 30°. Negative r/b_c values on the x-axis corresponds to locations below the lower side of the inclined ceilings.

2.2 Computational Domain and Mesh

The OpenFOAM version 2.3.x mesh generation utility, *snappyHexMesh*, is used for mesh generation [19]. The *snappyHexMesh* utility generates three-dimensional meshes primarily composed of hexahedral volumes. The current set of meshes has been generated with the inclusion of Stereolithography (STL) geometries of boxes, pallets and horizontal/inclined ceilings. The *snappyHexMesh* utility refines the background mesh to conform to the STL surfaces by an iterative refinement process (see [19] for details). Boundary layer addition is also included for the ceiling mesh with three layers of cells added beneath the ceiling surface (see Figure 2-5 and Figure 2-6). In the process of the fine mesh generation, besides hexahedral cells (which are divided into split-hexahedra), prismatic cells are also generated. Overall, the

percentage of prismatic cells is less than 3% of the total number of cells in any computational domain. On average, approximately 1.3 million cells are generated in a computational domain. The mesh resolution around the CUP rack-storage array was kept constant at $(0.025\ m)^3$ $((1\ in.)^3)$, whereas the uniform mesh below the ceiling (down to 0.3 m (12 in.)) was kept at a 0.1 m (4 in.) resolution. Four additional layers of non-orthogonal hexahedra with approximate volumes of $(0.1\ m)^3$ $((4\ in.)^3)$ were also present beyond the boundary layer mesh. The plume region mesh was kept at a fixed resolution of $(0.1\ m)^3$ $((4\ in.)^3)$ as well. It should be noted in Figure 2-6 that the "saw-tooth" mesh was avoided and the inclined ceiling at a 33.7° angle was resolved by the finite volume mesh. The number of mesh points in the transient boundary layer was approximately seven (with a 0.1 m resolution), which is comparable to the number of mesh points (approximately ten) used in the validation cases (with a 6.5 mm resolution).

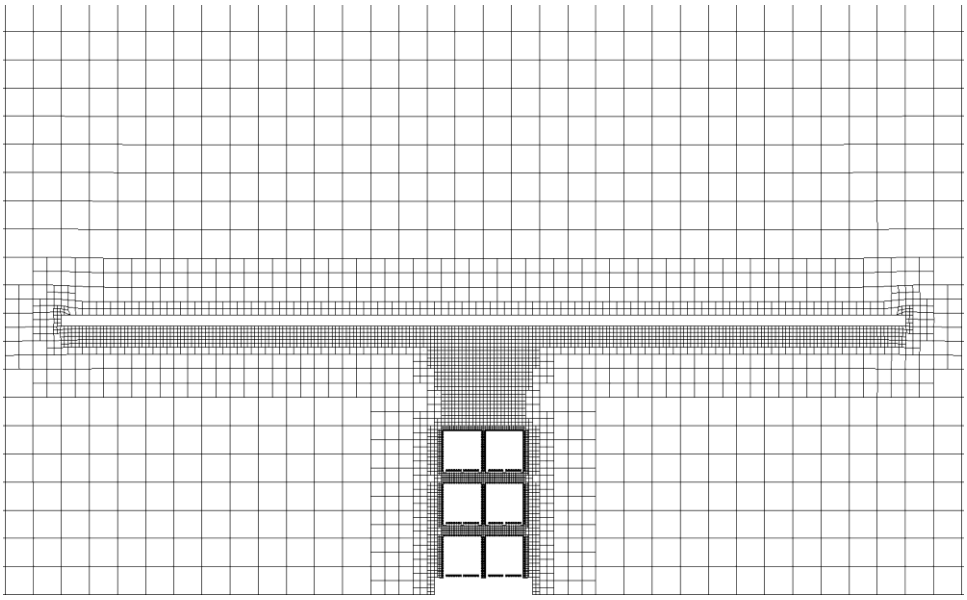

Figure 2-5: Computational mesh showing a ceiling inclined at 0° with its midpoint located 3.05 m (10 ft) above the CUP array. The mesh resolution in the boundary layer is held constant at 0.1 m (4 in.).

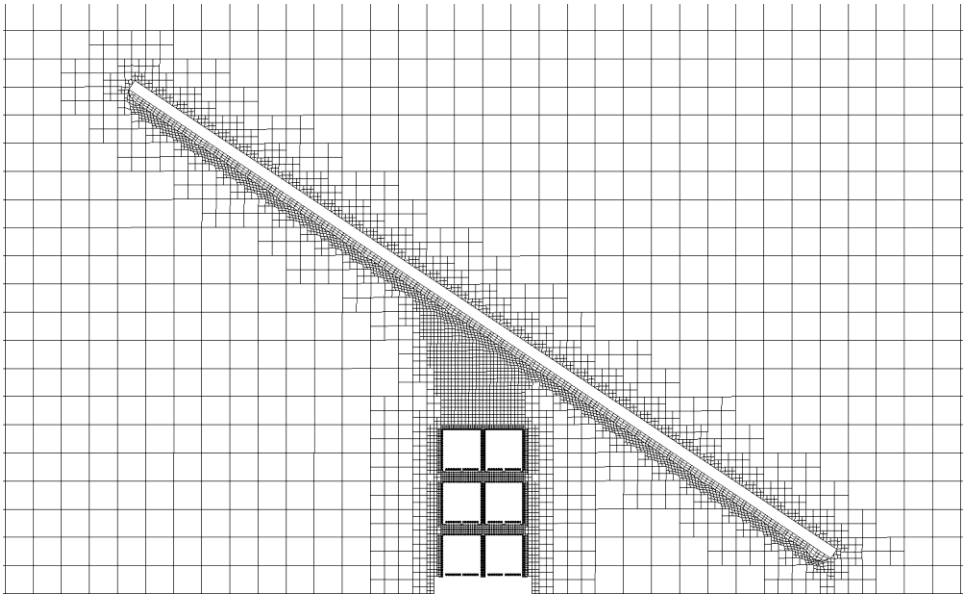

Figure 2-6: Computational mesh showing a ceiling inclined at 33.7° with its midpoint located 3.05 m (10 ft) above the CUP array. The mesh resolution in the boundary layer is held constant at 0.1 m (4 in.).

2.3 Fire Growth Modeling

The transient fire growth modeling over the CUP rack-storage array was conducted with the application of a recently developed pyrolysis model for the CUP commodity [31]. This pyrolysis model has been implemented in a development version of FireFOAM: the outer corrugated liner is simulated with the model developed earlier for corrugated pyrolysis [22] [23] [28], and the inner zone pyrolysis of corrugated and polystyrene is modeled using a lumped-mass approach (see [32] for details).

In order to expedite the simulation process in the present study, the new pyrolysis model [31] [32] is not directly applied. Instead, fire growth predictions were carried out using the full pyrolysis model and the resulting pyrolysis model output was saved. Then, for the sloped ceiling simulations a built-in "mapped" boundary method in OpenFOAM was used to map the stored pyrolysis model output, thus avoiding a repeat calculation of the pyrolysis model. This procedure is described below.

2.3.1 Mapping the Pyrolysis Boundary Condition

A mapping boundary condition, *timeVaryingMappedFixedValue*, which is available in OpenFOAM [18] was applied to map the pyrolysis boundary conditions. In order to generate the input values, the pyrolysis model [31] [32] was applied to simulate fire growth in a 2 x 2 x 3 CUP array in the absence of a ceiling and the mass fractions of the pyrolysis gases (corrugated and polystyrene), the surface temperature and mass flux (blowing velocity) distributions over the entire 2 x 2 x 3 boxes were spatially and temporally recorded at time intervals of 0.1 s for a total physical time of 150 s. A similar recording was made of the inputs from the wood pallets for the pyrolysate, temperature and velocity. A verification study of the mapping boundary condition was conducted. Reasonable agreement was found between the mapped boundary

condition and the full pyrolysis model, see Figure 2-7. Besides matching the HRR, comparisons of temperature and velocity fields in the plume region were also made.

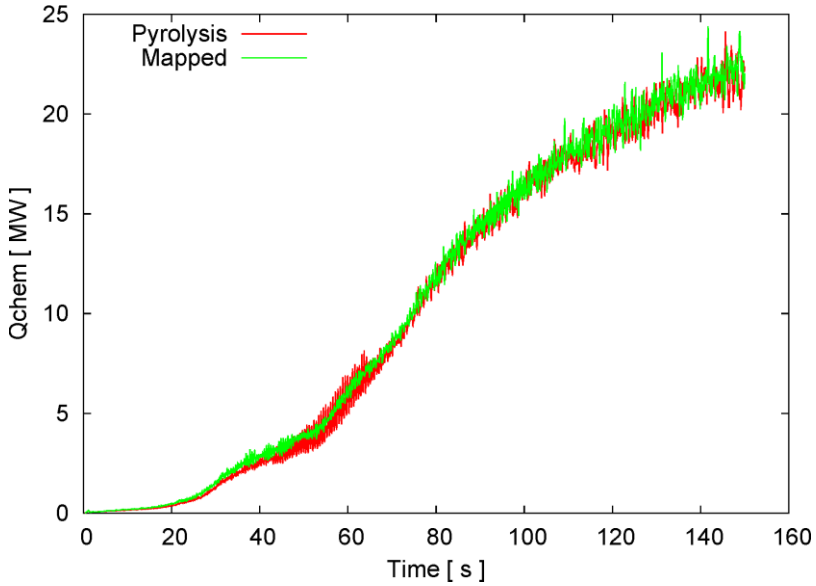

Figure 2-7: Chemical HRR computed using a pyrolysis model (red) and with the application of a mapped boundary condition (green).

2.3.2 Fire Growth Characteristics

Using the mapped boundary condition for pyrolysis, fire growth simulations under various ceiling configurations have been conducted. In Figure 2-8 instantaneous contours of the fire, represented by the stoichiometric mixture fraction value, are shown for three times. The 2 x 2 x 3 CUP rack-storage array is placed below a horizontal ceiling and the flames impinge on the ceiling at ~50 s. At 100 s, the entire second and third tiers of the array are engulfed by the fire and the flames spread below the ceiling. A larger flame footprint below the ceiling can be observed at 150 s. The fire chemical HRR reaches 25 MW at 150 s, as shown in Figure 2-9. The convective HRR peaks at approximately 15 MW at 150 s. The radiant fraction, also shown in Figure 2-9, varies with time, beginning with a 0.5 value for the igniter, then reducing down to ~0.22 for corrugated burning and finally increasing with increased burning of polystyrene.

The fire spread inside the CUP array was not perfectly symmetrical, due to the inclusion of two-way pallets that have larger open areas on two ends as compared to the other two ends. Close-up views of the pallet openings can be seen in Figure 2-10. Due to the larger pallet openings, the fire spread rate is faster along the y-direction, as is indicated by the wider fire size in Figure 2-10: at 60 s, the fire spread distance is approximately 33% greater, as inferred from measured flame widths. The effect of faster fire spread in one direction can be observed in the ceiling jet temperature contours and activation patterns discussed below.

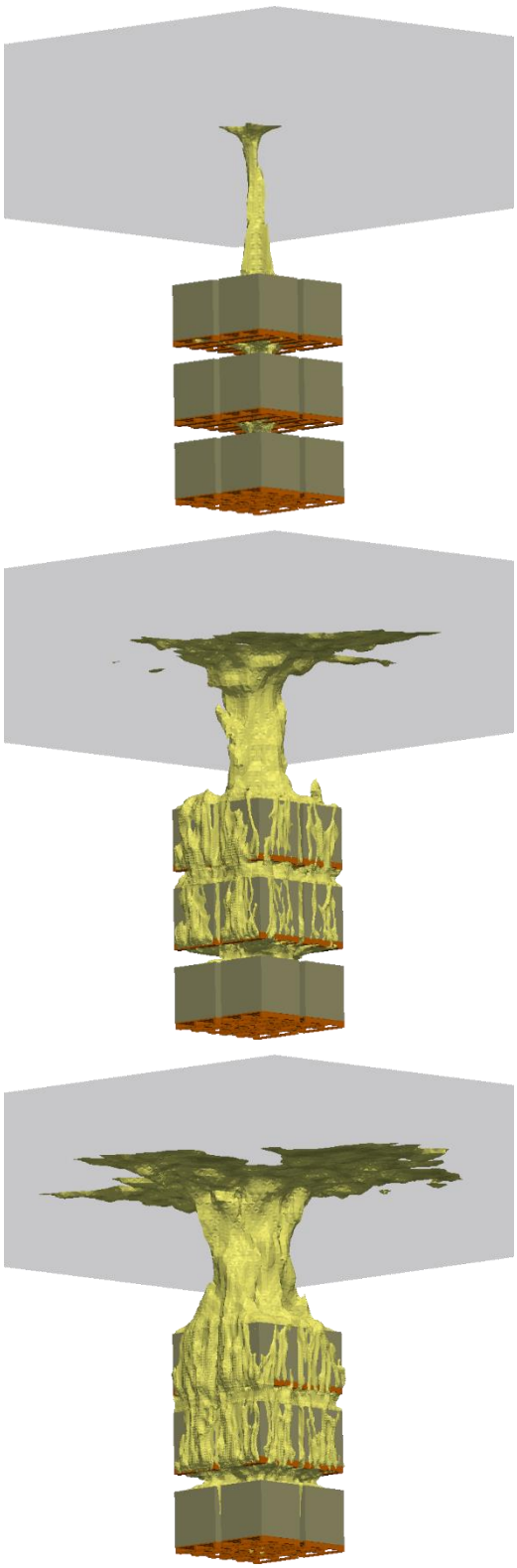

Figure 2-8: Snapshots of fire growth with the flame sheet depicted by the stoichiometric mixture fraction value. Flames impinge on a horizontal ceiling (0° inclination).

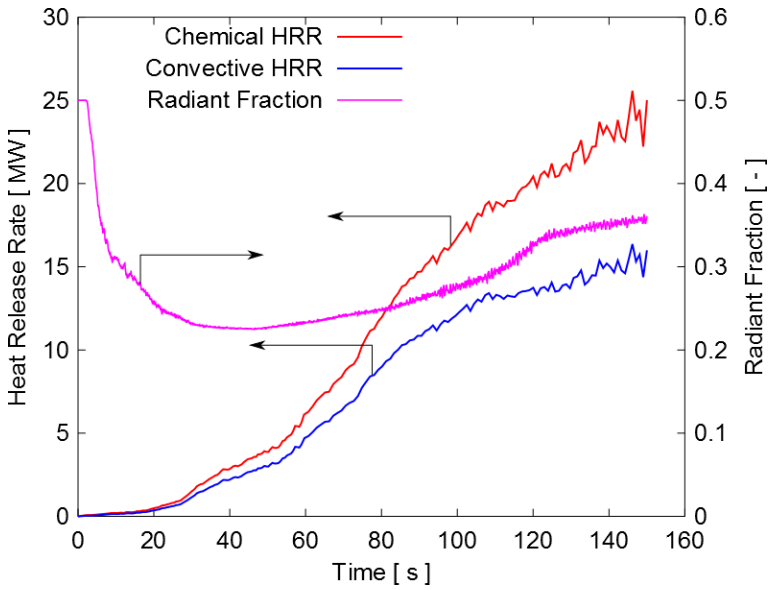

Figure 2-9: Modeled heat release rates (chemical and convective) and radiant fraction variation in time for 2 x 2 x 3 array of CUP commodity.

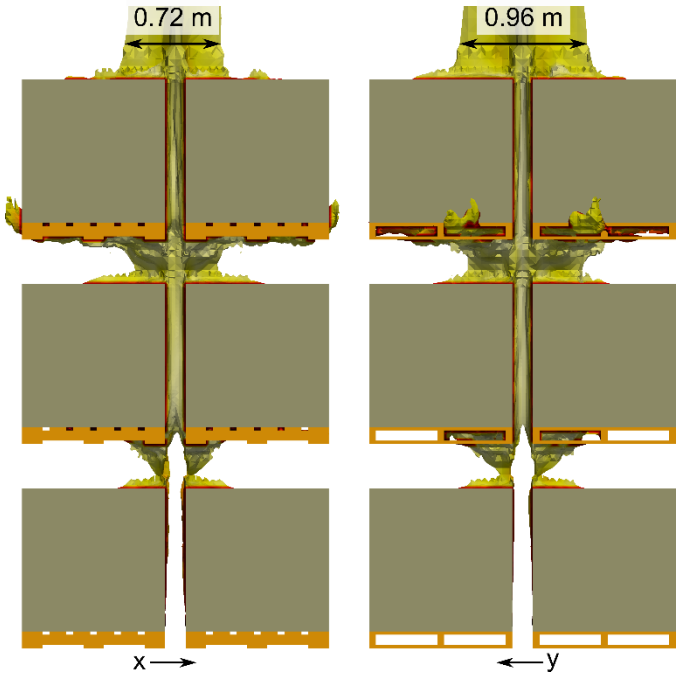

Figure 2-10: Snapshots of instantaneous flame-sheet depicted by the stoichiometric mixture fraction at 60 s after ignition. The fire in the flue spaces grows at a relatively faster rate in the y-direction.

2.4 Boundary Conditions

As described above, the pyrolysis region uses mapped boundary conditions for velocity, temperature and pyrolysate species. The ceiling was treated as an inert wall, with an isothermal temperature boundary (at 298.15 K) and a no-slip condition for velocity. The open boundaries on the sides were kept far away from the ceiling and rack-storage locations. The downstream outlet boundary was also kept sufficiently far away from the top of the inclined ceiling locations so as not to affect the flow.

2.5 Sprinkler Activation Setup

Sprinkler activations were simulated with calculations based on the RTI value. A scalar field variable for activation time, t_{act}, was developed to record activation times at each location in the computational mesh. Activation patterns based on the t_{act} distributions were extracted for the plane parallel to the inclined ceilings, located at a perpendicular distance of 0.33 m (13 in.) to the ceiling. These activation results provide detailed, spatial contours of activation times, as described in Section 3.

Activation times for a sprinkler layout corresponding to ignition among four sprinklers are also presented. These times were extracted by probing the t_{act} field at specified locations. Activation times for other sprinkler layouts (e.g., 8 ft x 12 ft or 2.4 m x 3.7 m) can be extracted in a similar way.

Two types of sprinklers were evaluated: the primary analysis was conducted with a quick-response sprinkler having an ordinary activation temperature (henceforth referred to as a QR/OT sprinkler) and for comparison purposes a standard response sprinkler with a high activation temperature (henceforth referred to as a SR/HT sprinkler) was also selected. The sprinkler characteristics were selected to cover the wide range of RTI and activation temperature combinations available for sprinklers in the industry. Details of the sprinklers are given in Table 2-2.

Table 2-2: List of sprinklers used in the present study.

Name	**Response**	**Activation Temperature** K (°F)	**RTI** $(m\text{-}s)^{0.5}$ $((ft\text{-}s)^{0.5})$	**C-Factor** $(m/s)^{0.5}$ $((ft/s)^{0.5})$
QR/OT	Quick	347 (165)	30 (54)	0.22 (0.40)
SR/HT	Standard	414 (286)	119 (216)	0.95 (1.72)

For the activation calculations, sprinkler sprays were not included, in order to isolate the activation patterns from suppression phenomena. This assumption was made since

- By excluding the sprays, the first-order effect of ceiling inclination on activation times and patterns can be studied.
- Accurately addressing suppression physics for the complex fire scenario considered here was beyond the scope of the study.
- In the case of ignition among four sprinklers, which would be the most conservative protection scenario for consideration, the impact of the sprays on the fire growth rate may not be very severe, at least for initial times.

2.6 Sprinkler Spray Setup

For the sprinkler spray simulations, a measured injection profile for a K200 lpm/bar$^{0.5}$ (K14.0 gpm/psi$^{0.5}$) pendent sprinkler reported in a previous study [17] has been applied. The injection profile was applied in the hemispherical region located 0.1 m (0.33 ft) below the sprinkler deflectors. This injection profile has been previously applied in suppression simulations [28]. Two scenarios have been simulated:

- One sprinkler above the ignition location – water mass flux distributions have been recorded 0.3 m (1 ft) above the CUP array with and without the presence of a 600 kW convective HRR fire source. The convective HRR was selected based on the first sprinkler activation time, as described below.
- Four sprinklers in an offset configuration around the ignition location (with a 3.05 m x 3.05 m or 10 ft x 10 ft spacing between them) – water flux distributions were recorded in the presence of a 2.6 MW convective HRR fire source. This activation scenario can be considered as the most conservative because the horizontal distance between the sprinkler and the fire location is the greatest.

3. **Sprinkler Activation Study**

Activations of sprinklers are simulated by decoupling sprinkler activation from the suppression physics. Activations caused by ceiling flows developing from the CUP rack-storage fire plume are simulated for five ceiling inclinations, from 0° to 33.7° angles. The flow characteristics, including temperature, are first described and profile changes with increasing inclination are discussed. Activation patterns and times for two types of sprinklers, quick-response, ordinary temperature (QR/OT) and standard-response, high temperature (SR/HT), are next presented and the recorded trends are discussed. The observations are summarized at the end of the section.

3.1 Ceiling Flows

3.1.1 Ceiling Jet Development

The transient plume originating from fire growth in the CUP rack-storage array results in the development of the thermal boundary layer below the ceiling. In Figure 3-1(a), instantaneous temperature contours are shown below a horizontal ceiling 3.05 m (10 ft) above the top of the CUP array. At early times, the fire height was observed to be smaller than the ceiling clearance and the hot gases in the plume resulted in a thin thermal boundary layer. With increasing time, the fire height becomes approximately equal to the ceiling clearance and the thickness of the boundary layer increases. Further increase in the boundary layer thickness occurs due to the widening of the plume attributed to the lateral fire spread on the CUP array. Overall, the flow below the horizontal ceiling can be observed to be symmetric in both directions.

For a ceiling inclined at 18.4°, the temperature profile at 100 s shows a skew towards the elevated side of the ceiling, as seen in Figure 3-1(b). The thermal boundary layer on the lower side of the ceiling reaches approximately 8 m (~26 ft) from the ceiling midpoint. In contrast, when the ceiling is inclined at 33.7° (Figure 3-1(c)), the thermal layer predominantly develops below the elevated side of the ceiling with the flow of hot gases below the lower side terminating around 4 m (~13 ft) from the ceiling midpoint. The ceiling jet thickness below the elevated side of the ceiling is observed to be greater compared to that for the 0° and 18.4° inclination cases.

Figure 3-2 includes instantaneous velocity vectors, colored by temperature, 100 s after ignition for the three ceiling inclinations of 0°, 18.4° and 33.7°. The velocity vectors for the 0° case are expectedly symmetrical as can be observed in Figure 3-2(a), whereas the velocities below the lower side decrease with increasing ceiling inclination, as can be observed in Figure 3-2(b) and (c).

The penetration distances along the ceiling slope for four inclinations, from 9.5° to 33.7°, are shown in Figure 3-3. The instantaneous penetration distances at 0.33 m (13 in.) perpendicular depth below the ceilings are non-dimensionalized using the ceiling half-width (12.2 m or 40 ft). For the 9.5° case, the penetration distance at 90 s reaches the ceiling end (a non-dimensional distance of unity). For the 18.4° case this distance increases from 0.4 at 30 s to ~1.0 at 150 s, whereas for the 26.6° and 33.7° inclinations, the penetration distance never exceeds 0.84 and 0.57, respectively.

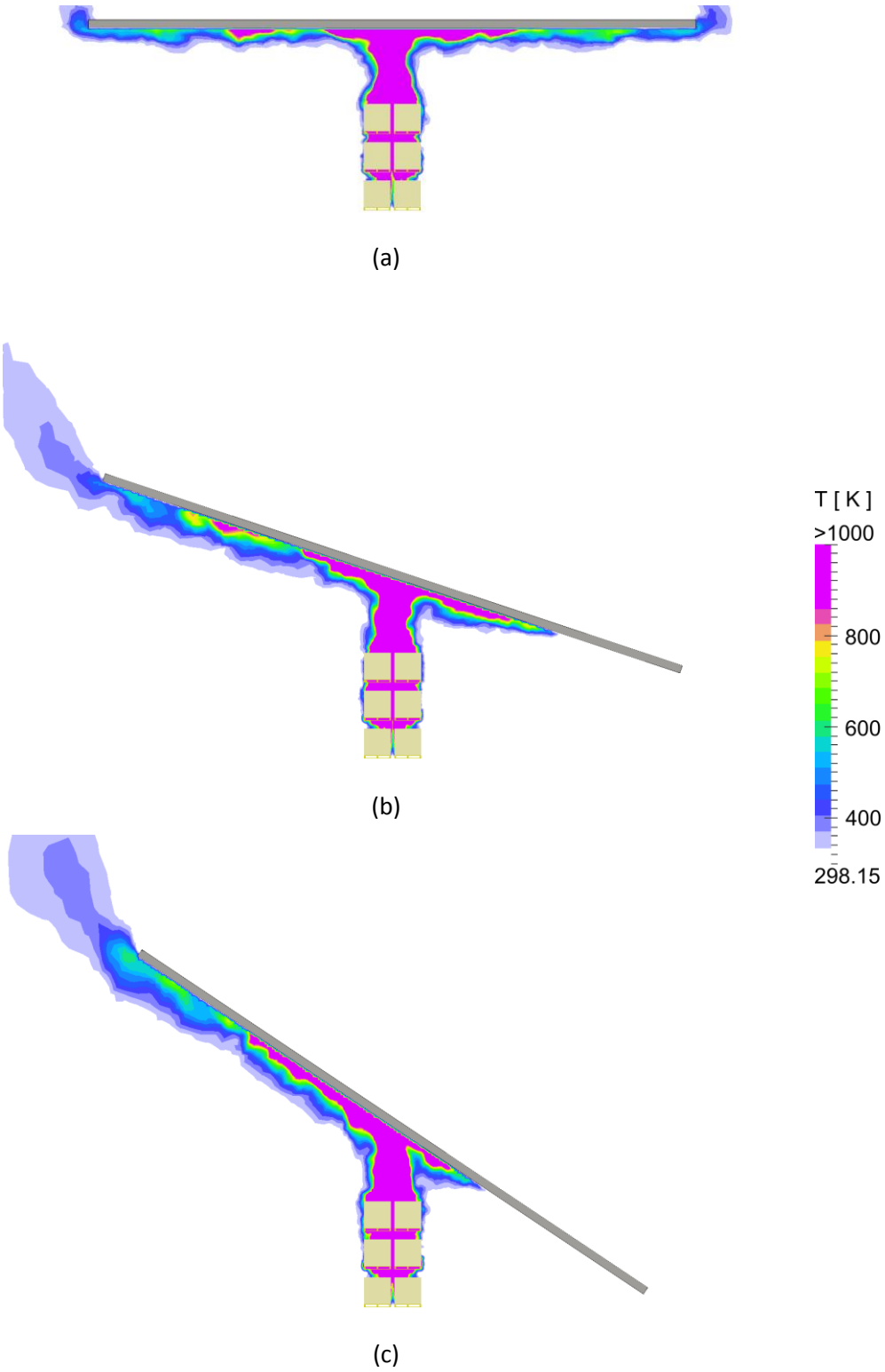

Figure 3-1: Instantaneous temperature snapshots at 100 s after ignition below ceilings with their midpoint 3.05 m (10 ft) above the CUP rack-storage array. Temperature contours shown for (a) 0°, (b) 18.4°, and (c) 33.7° inclinations.

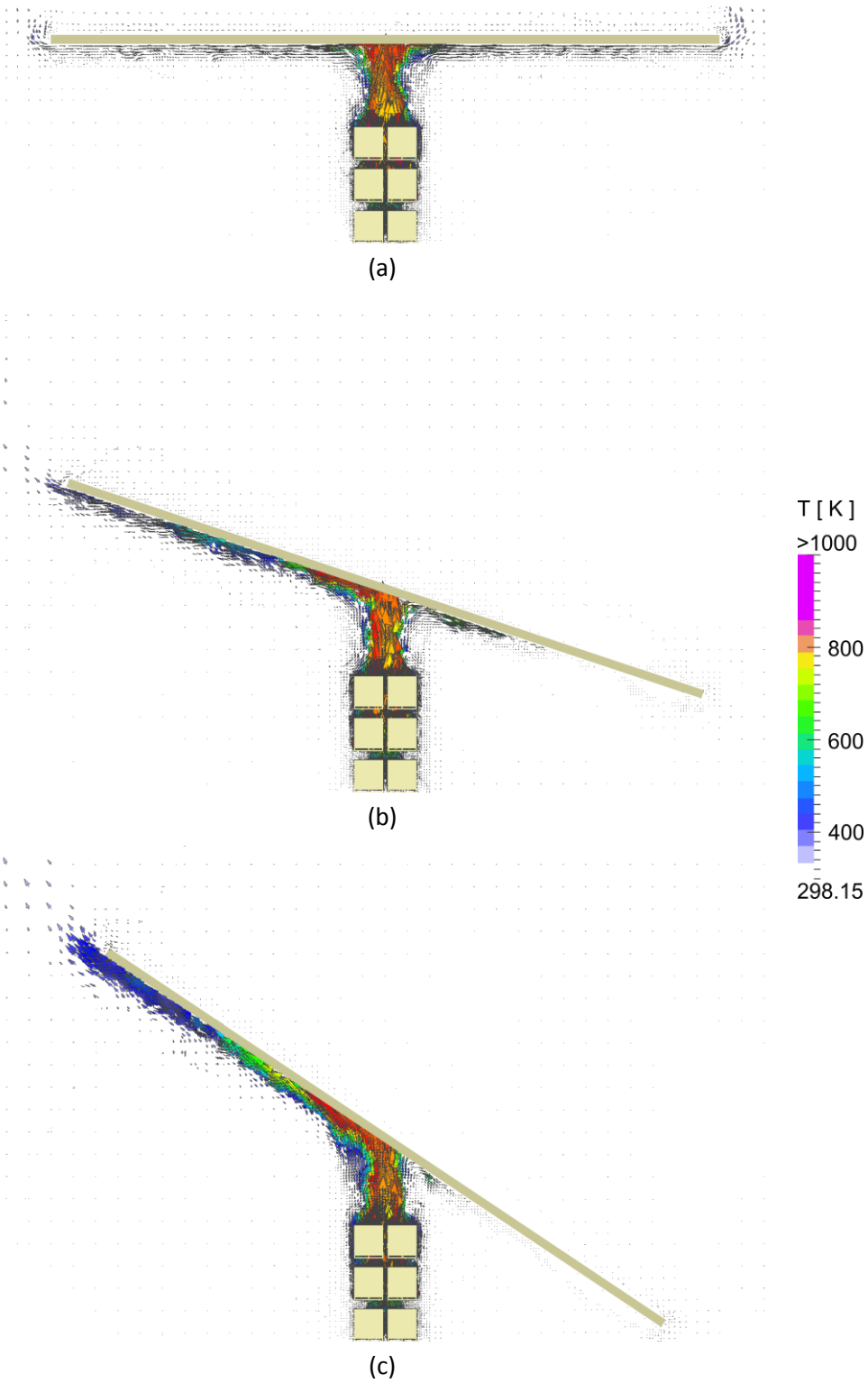

Figure 3-2: Instantaneous velocity vectors at 100 s after ignition below ceilings with their midpoint 3.05 m (10 ft) above the CUP rack-storage array. Vectors shown for (a) 0°, (b) 18.4°, and (c) 33.7° inclinations are colored by temperature.

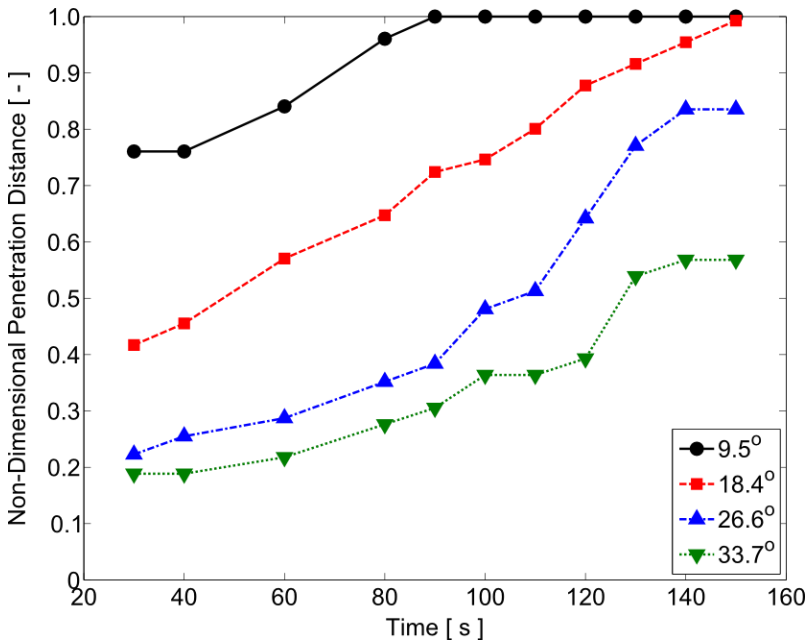

Figure 3-3: Non-dimensional penetration distances at 0.33 m (13 in.) perpendicular depth below the ceiling are plotted against time for four ceiling inclinations: 9.5°, 18.4°, 26.6° and 33.7°. The penetration distance is non-dimensionalized by the half-width of the ceiling (12.2 m or 40 ft).

3.1.2 Ceiling Jet Temperature Contours

Temperature contours 0.33 m (13 in.) below the ceiling are presented next. To facilitate comparison with thermocouple data, temperatures were recorded by modeling a K-type thermocouple with an RTI of 8.0 $(m\text{-}s)^{0.5}$ (14.5 $(ft\text{-}s)^{0.5}$). The profiles shown below provide an idea of the thermal boundary layer development as a function of time. The profiles also have a direct relation with the activation patterns of sprinklers as functions of time and inclination angle.

In Figure 3-4, temperature profiles below a horizontal ceiling are shown. Between 20 s and 80 s, a skewed development of the thermal layer can be observed. This is due to the asymmetric fire growth in the flue spaces of the CUP rack-storage array, as described earlier. The temperature profiles until 80 s show a bias towards the north and south directions (north is the direction of upwards incline for subsequent figures). For times >80 s, the temperature profile above the central ignition location becomes quite symmetric.

With the ceiling inclined at 18.4°, the developing temperature contours show skewed profiles towards the elevated side of the ceiling as shown in Figure 3-5. At 40 s, the temperature contours are wider on the elevated side. The ceiling jet is also wider (in the west-east directions) compared to the 0° case. For the 18.4° ceiling, the flow on the lower side turns back towards the elevated side of the ceiling. At times >80 s, the flow covers the entire elevated side of the ceiling. Higher temperature regions are present on both the elevated and lower sides. At 80 s, temperatures exceeding 500 K (440°F) extend to both the elevated and lower sides, but contours for temperatures >1000 K (1340°F) are mostly present on the elevated side, which indicates that the flames impinging on the ceiling turn upwards.

With the ceiling inclined at 33.7°, the ceiling jet predominantly forms on the elevated side. The flow turns upwards and at 40 s a much narrower ceiling jet is observed in Figure 3-6 compared to the one in Figure 3-5. It can be argued that the higher velocities present on the elevated side of the ceiling causes a narrower ceiling jet to develop. Only at later times (beyond 80 s), when the fire has engulfed the CUP rack-storage array and the plume has become wider, the ceiling jet widens to cover a substantial area beneath the elevated ceiling side.

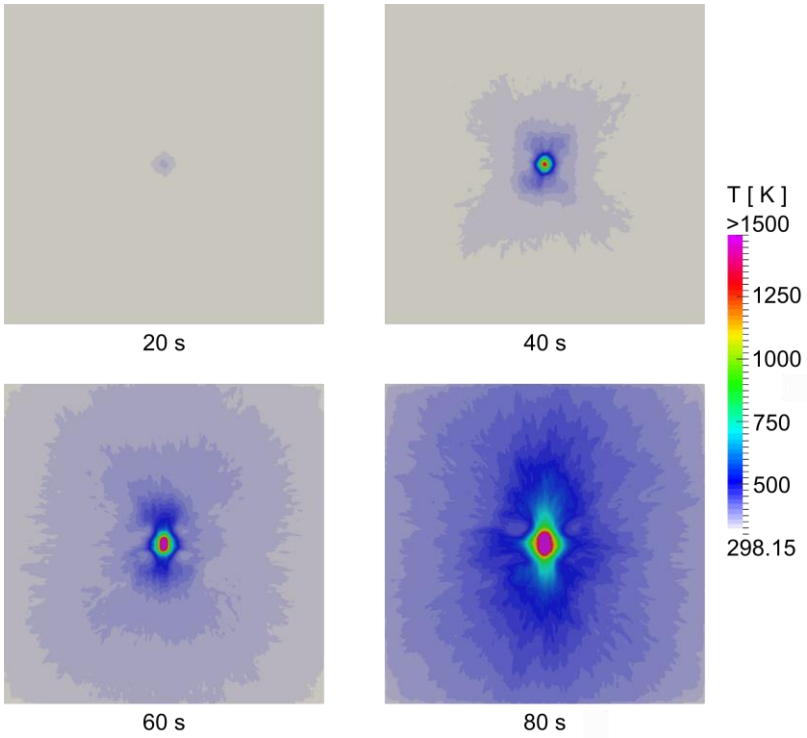

Figure 3-4: Computed temperature profiles 0.33 m (13 in.) below a horizontal 24 m x 24 m (80 ft x 80 ft) ceiling located 3.05 m (10 ft) above the CUP array.

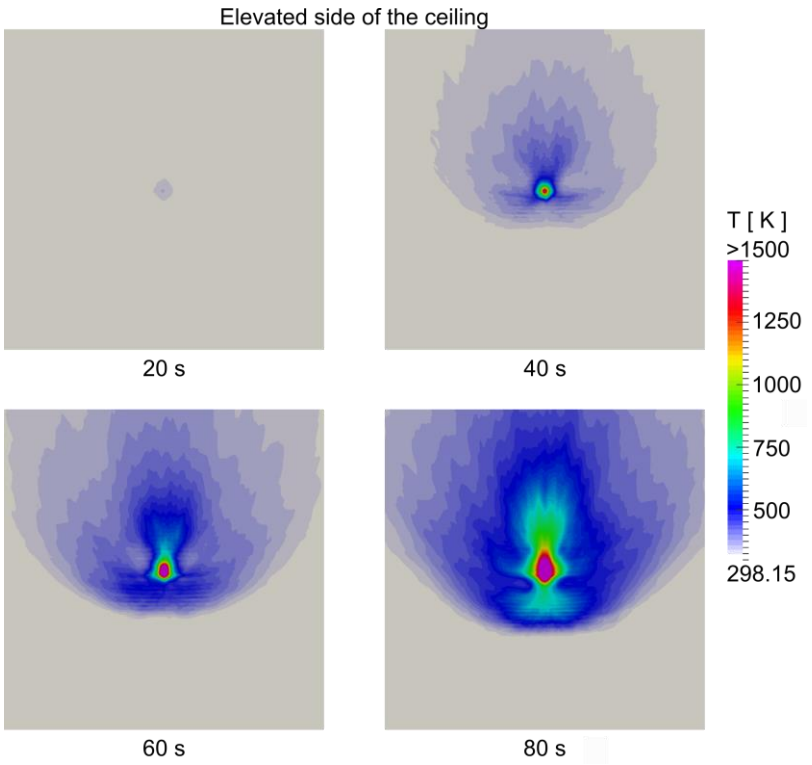

Figure 3-5: Computed temperature profiles 0.33 m (13 in.) below a 24 m x 24 m (80 ft x 80 ft) ceiling inclined at 18.4° with its midpoint located 3.05 m (10 ft) above the CUP array.

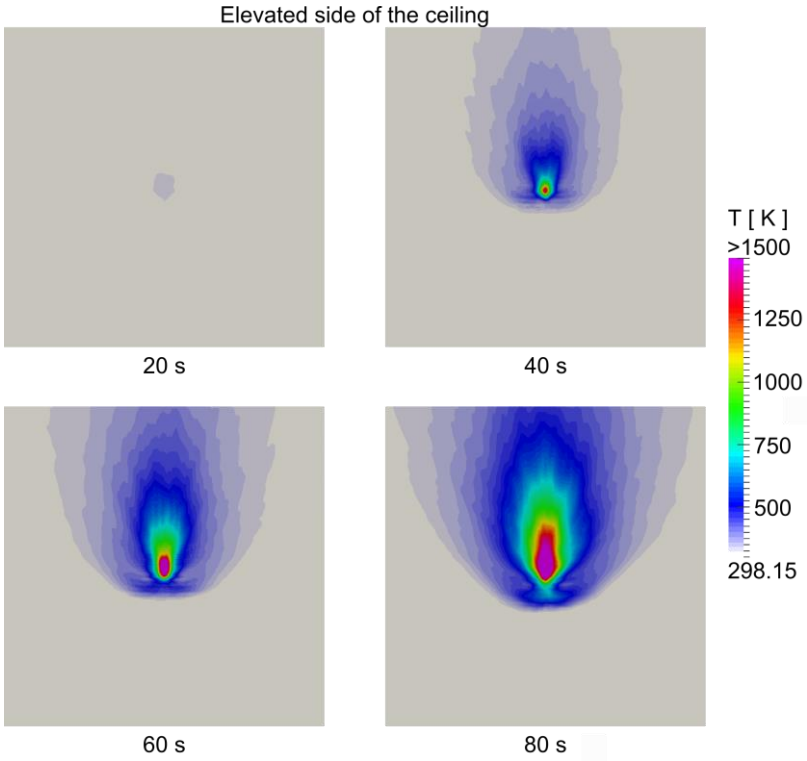

Figure 3-6: Computed temperature profiles 0.33 m (13 in.) below a 24 m x 24 m (80 ft x 80 ft) ceiling inclined at 33.7° with its midpoint located 3.05 m (10 ft) above the CUP array.

3.2 Activations of Quick-Response, Ordinary Temperature Sprinklers

Activation times and patterns are presented below for QR/OT sprinklers. The activation pattern can be inferred from the included contours of activation times. In addition, activation times are shown for a selected arrangement of sprinklers that ensures the ignition location is in the middle of four surrounding sprinklers (henceforth known as “among four sprinklers” configuration). The activation time contours shown in Figure 3-7 are for the case of a horizontal ceiling located 3.05 m (10 ft) above the top of the 2 x 2 x 3 CUP rack-storage array. As can be observed in Figure 3-7(a), the activation pattern is symmetric around the middle of the rack storage array, with earlier activation times observed in the north-south directions, due to reasons previously mentioned. The activation times are shown next to the sprinklers designated by the filled circles in the contour plots. In this arrangement, sprinklers would activate symmetrically around the rack-storage array, with the initial four activations occurring approximately around 49 s.

The number of activations plotted against activation time is shown in Figure 3-7(b) for the same sprinkler locations shown in Figure 3-7(a). The open circles in Figure 3-7(b) correspond to the sprinkler locations in the southward direction (below the ceiling midpoint location).

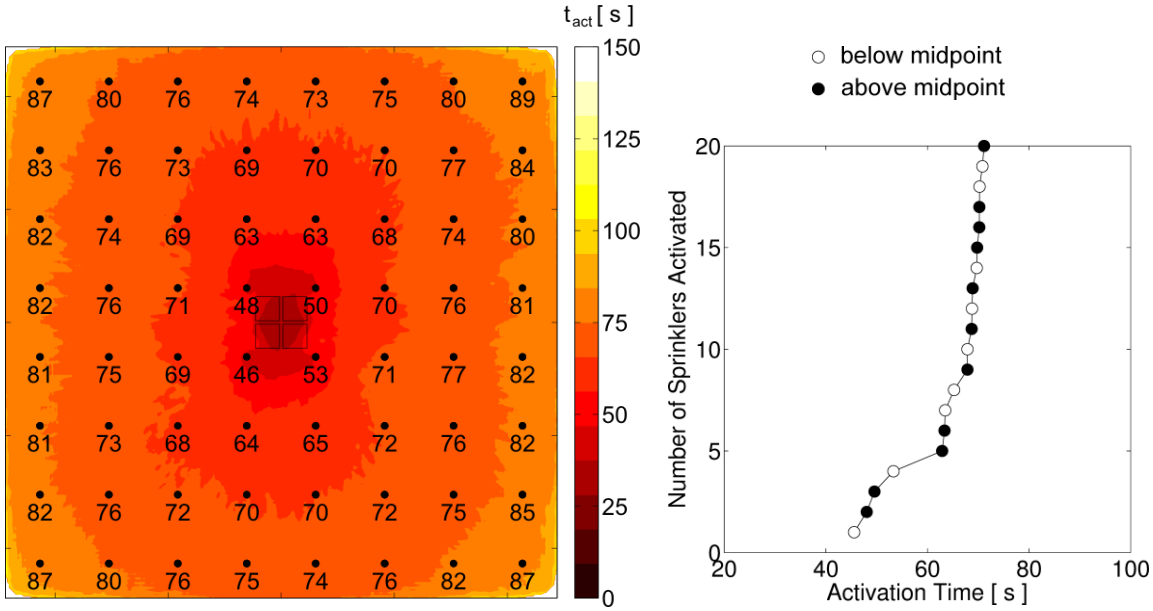

(a) (b)

Figure 3-7: Activation of QR/OT sprinklers located 0.33 m (13 in.) below a horizontal ceiling located 3.05 m (10 ft) above the CUP array: (a) activation time contours including filled circles indicating activated sprinkler locations when ignition is among four sprinklers. Predicted activation times are shown in seconds below the filled circles, and (b) number of sprinklers activated plotted against activation time.

For the same clearance (3.05 m or 10 ft), when the ceiling is inclined by 9.5°, the sprinkler activation pattern becomes biased towards the elevated side of the ceiling. Figure 3-8(a) shows the activation contours for the 9.5° inclination angle. The first four activations of sprinklers around the rack-storage array occur in an average time of approximately 49 s. This shows that the inclination of 9.5° would not significantly affect the first set of activations compared to activations under a horizontal ceiling. Figure 3-8(b) shows that after the initial set of activations, sprinklers in the elevated side activate in rapid succession, with several activations on the lower side occurring at later times. Similar to the 0° inclination case, the rate of sprinkler activations (Figure 3-8(b)) remains almost identical.

Similar trends are observed for an increase in the ceiling inclination to 18.4°. Significantly fewer activations occur on the lower side of ceiling in this case, as is shown in Figure 3-9(a). However, the four surrounding sprinklers still activate at reasonably close times, at an average time of 46 s. The rate of activations (Figure 3-9(b)), is lower compared to the 9.5° inclination case. For an 18.4° ceiling inclination, early and symmetric activations of sprinklers surrounding the ignition location will occur. Fewer further activations will occur on the lower side of the ceiling.

At a 26.6° inclination, the trend of activating the elevated-side sprinklers is even more pronounced. The majority of activations occur below the elevated side of the ceiling, as can be observed in Figure 3-10(a). Although the average time of activations of the four sprinklers surrounding the ignition location (46 s) remains the same as for the 18.4° inclination case, the difference between activation times for the two elevated sprinklers and the two lower sprinklers increases from an average of 3.5 s for the 18.4° case to 16.5 s. This time difference is an indication that flows developing below ceilings with inclinations ≥26.6° will be greatly skewed towards the elevated side so as to result in delayed activation of sprinklers on the lower side of the ceiling. This observation is valid for ceiling flows resulting from the initial fire growth in a region located among four sprinklers. Compared to the 18.4° case, the sprinkler activation rate reduces further for the 26.6° inclination ceiling, with fewer activations occurring at large intervals, as can be seen in Figure 3-10(b).

Increasing the inclination to 33.7° causes the activation of sprinklers to occur primarily on the elevated side, with the first sprinkler activation on the lower side occurring 28 s after first activation, as seen in Figure 3-11(a). The overall coverage area for activations is also observed to have shrunk considerably compared to the 26.6° case. In this scenario, the outermost sprinklers have not activated in the first 150 s. The slope of the number of activations in Figure 3-11(b) is also the lowest compared to the other cases, with long delays observed at later times. Rapid activations can also be observed to occur in a narrow region below the elevated side.

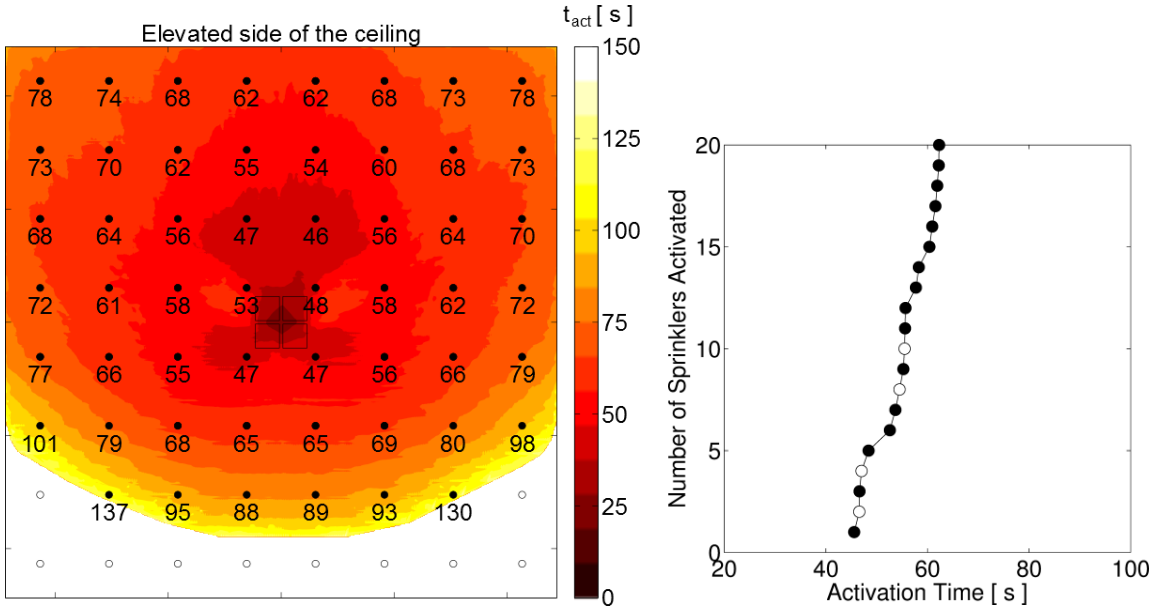

(a) (b)

Figure 3-8: Activation of QR/OT sprinklers located 0.33 m (13 in.) below a ceiling inclined at 9.5° with its midpoint located 3.05 m (10 ft) above the CUP array: (a) activation time contours, and (b) number of sprinklers activated plotted against activation time.

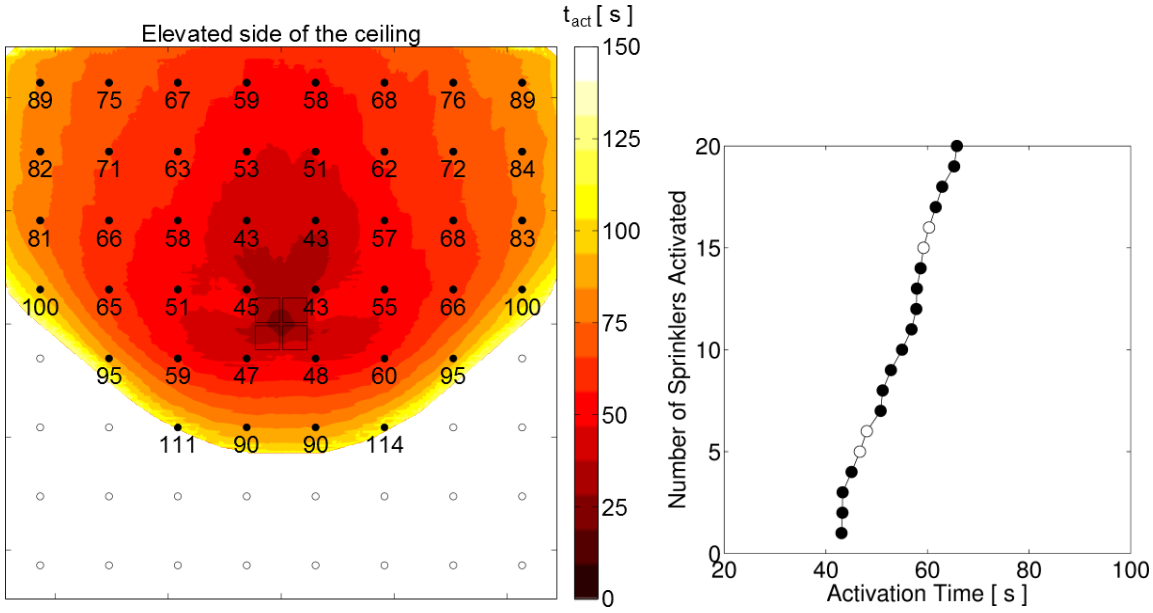

(a) (b)

Figure 3-9: Activation of QR/OT sprinklers located 0.33 m (13 in.) below a ceiling inclined at 18.4° with its midpoint located 3.05 m (10 ft) above the CUP array: (a) activation time contours, and (b) number of sprinklers activated plotted against activation time.

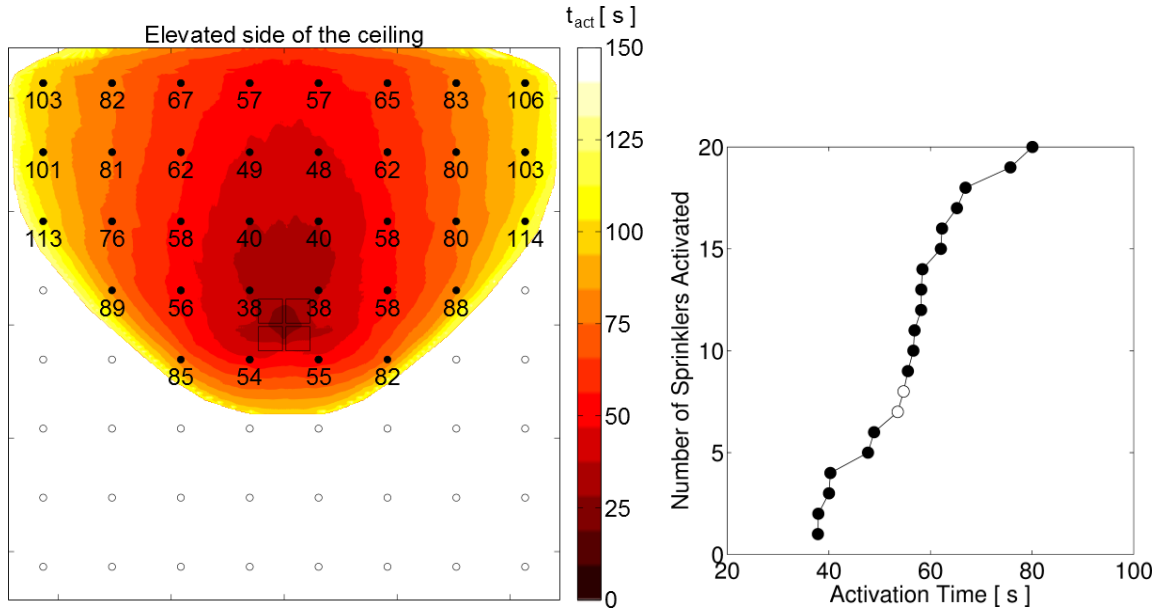

(a) (b)

Figure 3-10: Activation of QR/OT sprinklers located 0.33 m (13 in.) below a ceiling inclined at 26.6° with its midpoint located 3.05 m (10 ft) above the CUP array: (a) activation time contours, and (b) number of sprinklers activated plotted against activation time.

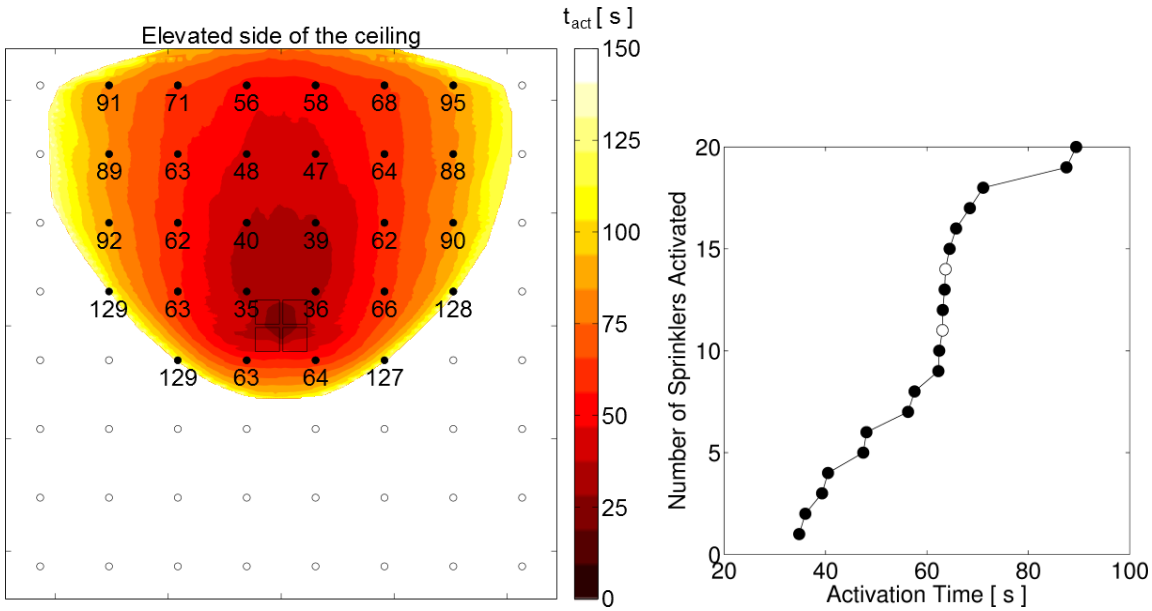

(a) (b)

Figure 3-11: Activation of QR/OT sprinklers located 0.33 m (13 in.) below a ceiling inclined at 33.7° with its midpoint located 3.05 m (10 ft) above the CUP array: (a) activation time contours, and (b) number of sprinklers activated plotted against activation time.

From this part of the study, it can be concluded that for QR/OT sprinklers,

- with increasing ceiling inclination, sprinkler activation patterns tend to become increasingly skewed towards the elevated side of the ceilings,
- the delay in activations between sprinklers located below the elevated and lower sides of the ceilings increases with increasing inclination, and
- the results show that, for the fire hazard that is under evaluation, ceilings up to and including 18.4° inclination have similar activation times and patterns as horizontal ceilings for the four sprinklers immediately adjacent to the fire source.

3.3 Activation of Standard-Response, High Temperature Sprinklers

For standard-response, high temperature (SR/HT) sprinklers, the activation patterns are presented and activation times are compared with the QR/OT times. In Figure 3-12(a), the activation pattern for a horizontal ceiling is shown. Unlike the QR/OT activation pattern, the SR/HT pattern is confined to a smaller region below the ceiling. The activations are delayed with the first occurring later than 50 s compared to the first QR/OT activation. This difference would provide a greater suppression challenge and control of fire spread would be more difficult. From Figure 3-12(b) we can notice the significant initial activation delay and the slower rate of activations for the SR/HT sprinklers compared to the QR/OT sprinklers.

For a ceiling inclined at 18.4°, Figure 3-13(a), the initial activation delay compared to the QR/OT sprinklers is less than 30 s. However, compared to the QR/OT pattern, the sprinklers closest to the CUP array on the lower side operate with a much longer delay. In the case of the QR/OT sprinklers, the four sprinklers surrounding the CUP array would activate almost simultaneously. Compared to the horizontal ceiling case, the two SR/HT sprinklers on the lower side adjacent to the ignition location activate earlier. In Figure 3-13(b) it can be observed that the rate of activations in the case of SR/HT sprinklers is approximately constant and equal to the QR/OT activation rate, but with an initial delay of approximately 30 s.

As in the case of QR/OT sprinklers, for a ceiling inclined at 33.7°, the SR/HT sprinklers closest to the CUP array on the lower side of the ceiling will operate with a delay of approximately 74 s compared to the closest sprinklers on the elevated side as observed from Figure 3-14(a). This time difference increases for SR/HT sprinklers compared to the delay for QR/OT sprinklers (approximately 28 s). The activations for the SR/HT sprinklers also occur in a narrower region, predominantly below the elevated side of the ceiling. In Figure 3-14(b), apart from the initial delay of the first activation, the slope of initial activations for the SR/HT sprinklers remain almost equal to the initial QR/OT slope.

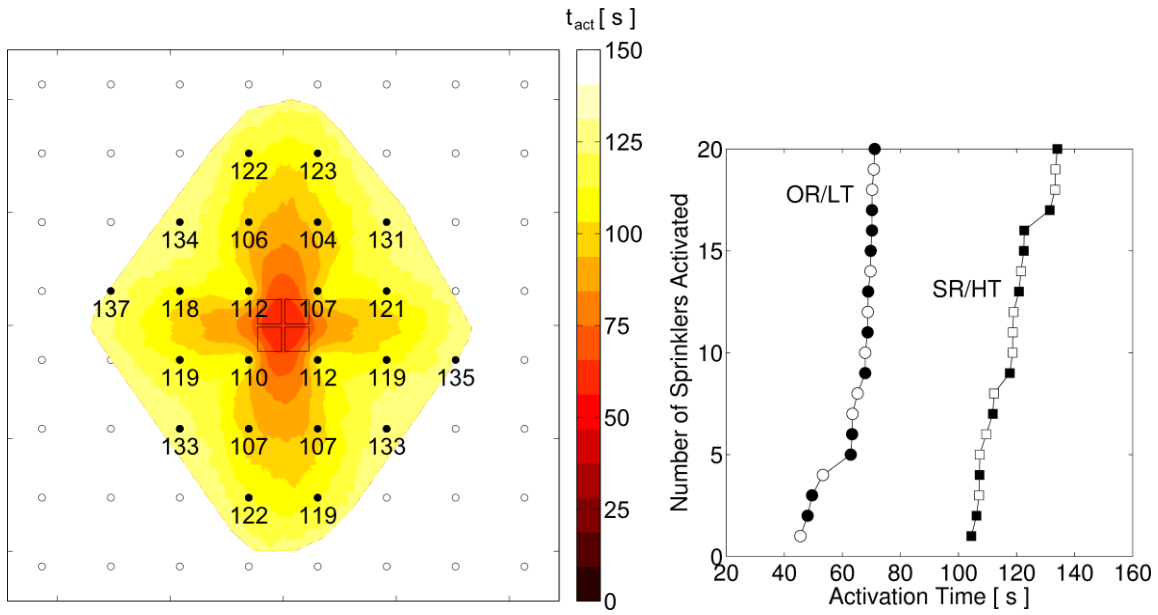

(a) (b)

Figure 3-12: Activation of SR/HT sprinklers located 0.33 m (13 in.) below a horizontal ceiling located 3.05 m (10 ft) above the CUP array: (a) activation time contours including filled circles indicating activated sprinkler locations when ignition is among four sprinklers are shown, and (b) the number of sprinklers activated is plotted against activation time for the SR/HT and QR/OT sprinklers.

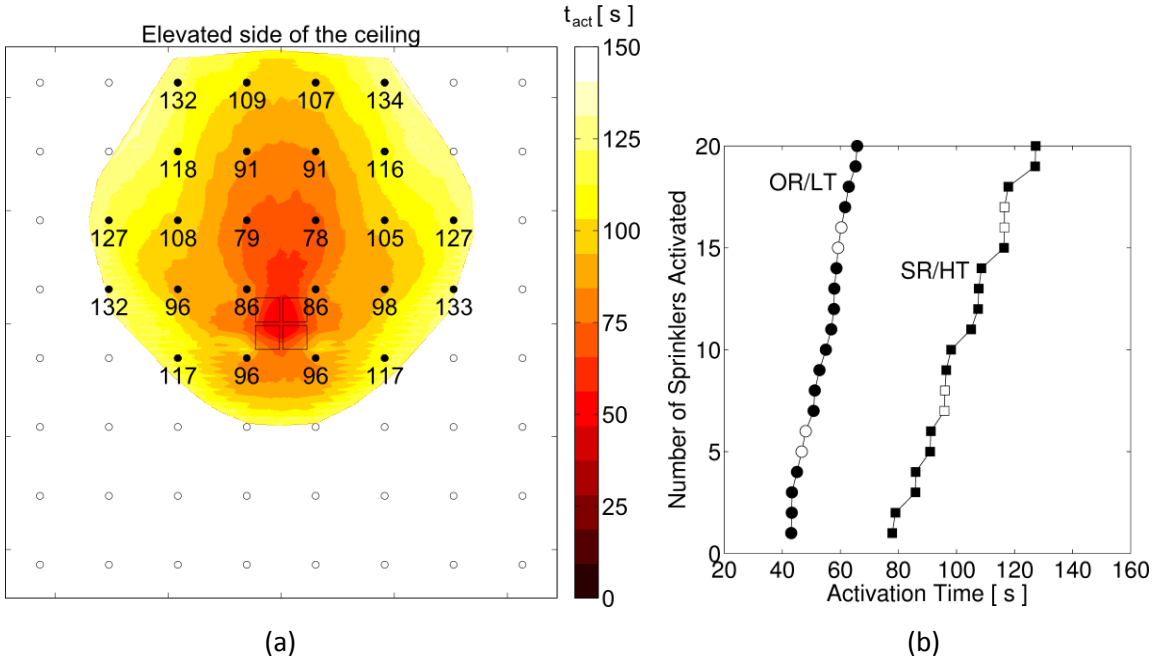

(a) (b)

Figure 3-13: Activation of SR/HT sprinklers located 0.33 m (13 in.) below a ceiling inclined at 18.4° with its midpoint located 3.05 m (10 ft) above the CUP array: (a) activation time contours, and (b) the number of sprinklers activated is plotted against activation time for the SR/HT and QR/OT sprinklers.

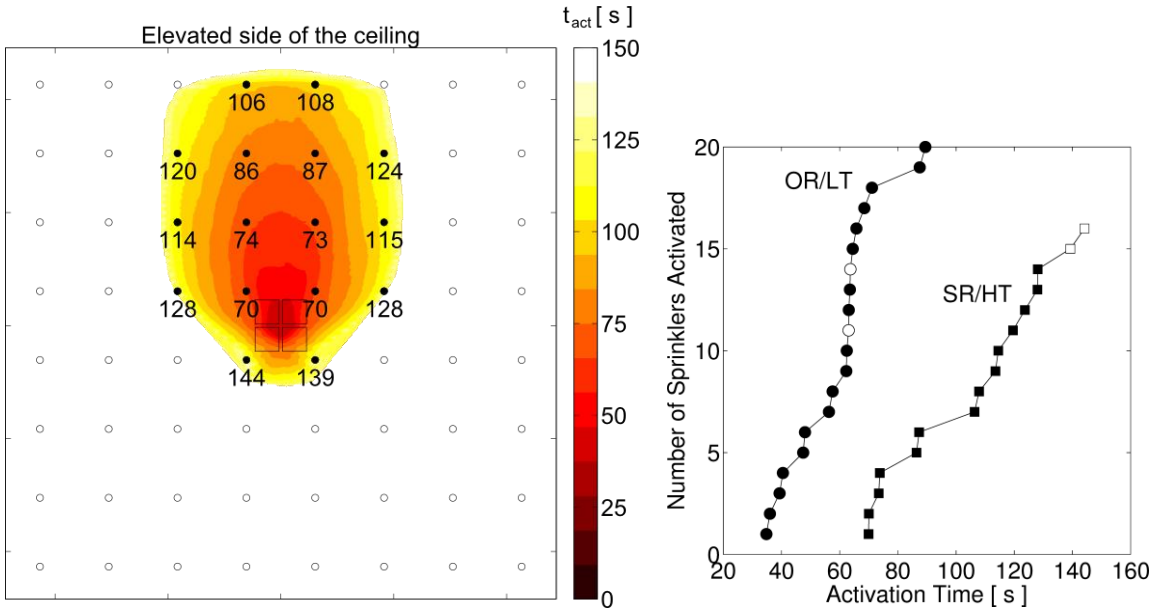

(a) (b)

Figure 3-14: Activation of SR/HT sprinklers located 0.33 m (13 in.) below a ceiling inclined at 33.7° with its midpoint located 3.05 m (10 ft) above the CUP array: (a) activation time contours, and (b) the number of sprinklers activated is plotted against activation time for the SR/HT and QR/OT sprinklers.

Based on the simulation results for SR/HT sprinklers, the following can be concluded:

- the average delay time for activations significantly increases when compared to QR/OT,
- the closest sprinklers around the ignition location showed an increase in activation time difference between the elevated and lower side sprinklers, and
- also, several additional activations take place on the elevated side before the two sprinklers below the lower side activate.
- Therefore, if using SR/HT sprinklers, the impact of sloped ceiling on activation time and pattern is greater when compared to QR/OT sprinklers.

3.4 Effect of Ceiling Clearance

For 18.4°, increasing the ceiling clearance from 3.05 m (10 ft) to 6.1 m (20 ft) results in a wider region of activation locations, as shown in Figure 3-15(a). The increased plume width below the ceiling causes a wider spread of the ceiling jet. The total number of activations also increases on the lower side of the ceiling.

The average time difference between the first two activations of QR/OT sprinklers on the elevated side and the first two activations on the lower side is ~9 s, compared to ~3.5 s for the 3.05 m (10 ft) clearance. This difference is much smaller than the differences for 26.6° and 33.7° inclined ceilings with 3.05 m (10 ft) clearances – 16.5 s and 28 s, respectively. Average activation times for the first four QR/OT sprinklers surrounding the ignition location increases to 48.5 s for the 6.1 m (20 ft) clearance compared to 45.8 s for the 3.05 m (10 ft) clearance. For SR/HT sprinklers, the average activation times are higher, 87.2 s and 92.6 s for the 3.05 m (10 ft) and 6.1 m (20 ft) clearances, respectively. The activation rate slopes for QR/OT sprinklers remain similar for both the clearances (see Figure 3-15(b)). However, for SR/HT sprinklers the slope for the 6.1 m (20 ft) clearance case is greater. It is expected that, for a ceiling clearance of less than 3.05 m (10 ft), the activation pattern and times of QR/OT sprinklers below 18.4° inclined ceilings will show trends similar to those seen in Figures 3-9 and 3-15.

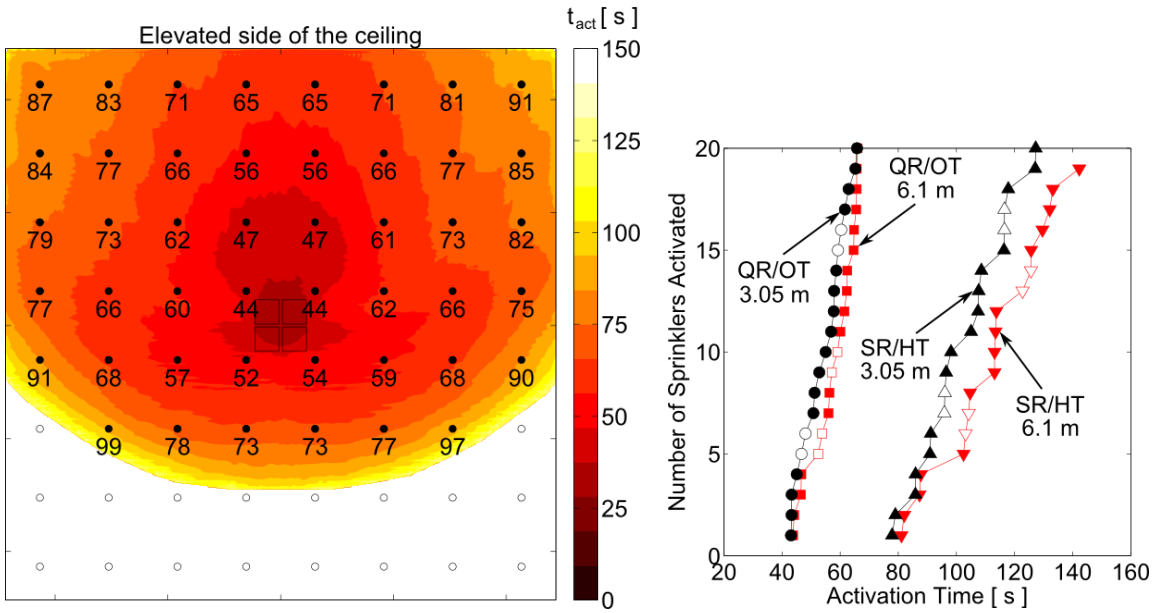

(a) (b)

Figure 3-15: Effect of ceiling clearance: (a) activation time contours of QR/OT sprinklers located 0.33 m (13 in.) below a ceiling inclined at 18.4° with its midpoint located 6.1 m (20 ft) above the CUP array, and (b) number of sprinklers activated plotted against activation time: round symbols correspond to QR/OT sprinklers, 3.05 m (10 ft) clearance, square symbols are for QR/OT sprinklers, 6.1 m (20 ft) clearance and the triangles and inverted-triangles are for SR/HT sprinklers below 3.05 m (10 ft) and 6.1 m (20 ft) ceilings, respectively.

3.5 Summary

Based on the activation simulations involving QR/OT sprinklers, the results show that ceilings up to and including 18.4° inclination have similar activation times and patterns as horizontal ceilings for the four sprinklers immediately adjacent to the fire source. For this inclination, symmetric activation of sprinklers would take place in the first ring around the ignition location with only a 3.5 s differential between the elevated and lower side activations. Increasing the inclination to 26.6° and above would produce significant delays in activations on the lower side of the ceiling: the time difference increases to 16.5 s for a 26.6° inclination and to 28 s for a 33.7° inclination. The number of sprinklers activated on the elevated side also greatly exceeds the number of activations on the lower side when the ceiling inclination is greater than 18.4°.

If SR/HT sprinklers are used, the average delay time for activations of the four sprinklers surrounding the ignition location increases to 10 s for the 18.4° inclination case. Four more activations take place in the elevated section before the sprinklers on the lower side activate, indicating the activation pattern skewness is accentuated with the use of the SR/HT sprinklers.

In the present study, when the ceiling clearance is increased from 3.05 m (10 ft) to 6.1 m (20 ft), the average activation time for the four sprinklers surrounding the ignition location increased by ~3 s and ~5 s for QR/OT and SR/HT sprinklers, respectively. Such activation time delays may have an adverse impact on protection design.

4. **Sprinkler Sprays Study**

In order to understand the effect of ceiling slope and deflector orientation, sprinkler spray simulations are conducted. Two scenarios are considered: when a single sprinkler activates above the CUP rack-storage array and when four sprinklers operate together. The ceiling clearance for the spray calculations is 3.05 m (10 ft) from the top of the CUP array to the ceiling midpoint. Consideration is also given to the two deflector orientations that are predominantly used in industrial facilities – deflector parallel to the floor or to the ceiling.

For the single sprinkler part of the study, comparisons are also made between when the fire plume is present and for cold flow simulation results. The role of the fire plume in spray penetration becomes clearer by comparing the fire cases with the no-fire cases. For each case, spray calculations are conducted for a duration of 30 s and the collected water flux distribution 0.3 m (1 ft) above the CUP array is averaged for the last 20 s of the simulations. The water flux is recorded at an array of 0.61 m x 0.61 m (2 ft x 2 ft) sampling areas covering a total area of ~149 m^2 (1600 ft^2). Comparison is also made between cases by integrating the water flow rate for a 3.05 m x 3.05 m (10 ft x 10 ft) area above the CUP array. This area is assumed to cover the region where fire growth is taking place and also where pre-wetting would be required to successfully control lateral fire spread in neighboring storage arrays.

4.1 Sprinkler Selection

A K200 lpm/$bar^{0.5}$ (K14.0 gpm/$psi^{0.5}$) ESFR pendent sprinkler was used for this study employing the spray measurements of Zhou et al. [17]. The water pressure for the spray calculations is held constant at 3.4 bar (50 psi).

4.2 Selection of Heat Release Rates

For the one sprinkler case, the activation time of the QR/OT sprinkler was found to be approximately 25 s irrespective of the ceiling orientation. The convective HRR at 25 s is approximately 600 kW. The fire convective HRR was therefore kept constant at 600 kW for the single sprinkler spray calculations.

In the case of spray simulations involving four sprinklers, for a horizontal ceiling the first four sprinklers to activate were located around the CUP rack-storage array. In the case of the 18.4° inclined ceiling, considering the minor time differences between the first six activations, the four sprinklers surrounding the CUP array were also selected for the spray calculations. The first four activations when the ceiling was inclined at 33.7° occurred on the elevated side of the ceiling. The selected sprinklers for spray calculations are shown in Table 4-1 along with the average activation times for the four sprinklers and the corresponding convective HRR. For consistency, the convective HRR for each spray calculation was held constant at 2.6 MW, which was an average of the convective HRRs shown in Table 4-1. This way the plume strength was kept fixed and comparison of collected water flux above the CUP rack-storage array could be made for the different inclination cases.

Table 4-1: Sprinkler activation times, average activation time (t_{avg}) for four sprinklers selected for spray calculations, and the convective HRR at t_{avg}. The selected sprinklers for spray calculations are enclosed by the red square.

Ceiling Inclination	0°	18.4°	33.7°
		Elevated side	
Sprinkler Activation Times (s)	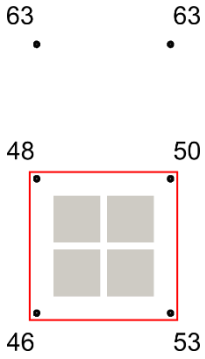	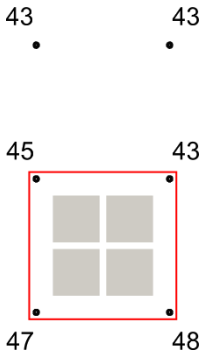	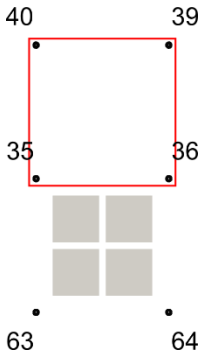
Average Activation Time, t_{avg} (s)	49	46	38
Convective HRR at t_{avg} (MW)	3.0	2.7	2.1

4.3 Water Flux Distributions from One Sprinkler

When the ceiling is not inclined, the sprinkler deflector is always parallel to the floor and the spray core from the K200 (K14) impinges on the fire plume. An instantaneous snapshot of sprinkler spray for the 0° inclination case is shown in Figure 4-1(a).

For an inclination of 18.4° and parallel-to-floor deflector orientation, the spray is primarily directed downwards, except in a short section of the lower side of the ceiling where the spray impinges on the ceiling. The impingement can be observed in Figure 4-1(b). The impinging droplets are simulated to rebound in an inelastic manner. In this case, a total of 4.4% of water mass injected from the sprinkler impinges on the ceiling. With the ceiling at 18.4° and parallel-to-ceiling orientation, such impingement on the lower side of the ceiling is not observed, see Figure 4-1(c). However, in this case, the central spray core is perpendicular to the ceiling and tends to deposit water away from the ignition location where the fire is present.

When the ceiling is inclined at 33.7° and for the parallel-to-floor orientation, the spray impingement on the lower side of the ceiling becomes even more severe, as is noticeable in Figure 4-1(d). The fraction of water impinging on the ceiling is 13.2% of the total water mass injected. For the parallel-to-ceiling orientation (Figure 4-1(e)), the central spray core travels further away from the fire growth region and the plume penetration capability of the spray is reduced, as will be shown below.

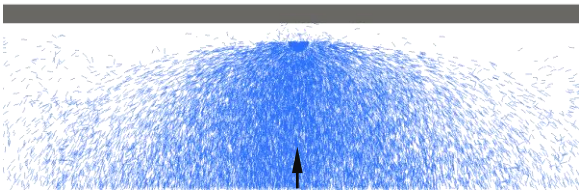

(a) 0°, deflector parallel to floor

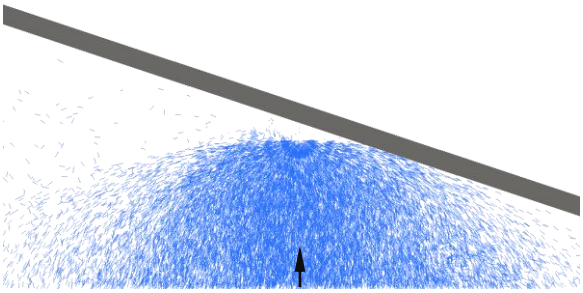

(b) 18.4°, deflector parallel to floor

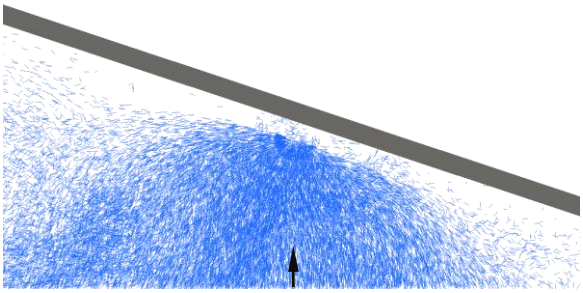

(c) 18.4°, deflector parallel to ceiling

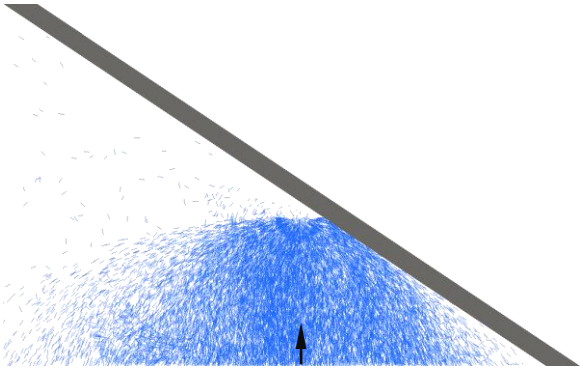

(d) 33.7°, deflector parallel to floor

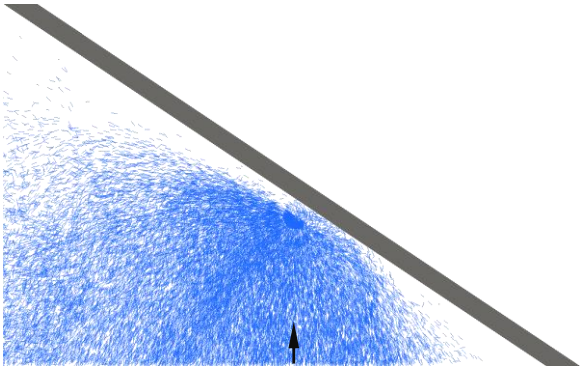

(e) 33.7°, deflector parallel to ceiling

Figure 4-1: Instantaneous snapshots of sprays originating from the K200 (K14) sprinkler for (a) 0° inclination, deflector parallel to floor, (b) 18.4° inclination, deflector parallel to floor, (c) 18.4° inclination, deflector parallel to ceiling, (d) 33.7° inclination, deflector parallel to floor, and (e) 33.7° inclination, deflector parallel to ceiling. A fire plume of 600 kW convective HRR was present. Plume centerline is shown by the vertical arrows.

The droplet mass flux distribution at a collection plane 0.3 m (1 ft) above the CUP rack-storage array is presented below. Water mass is collected at the 0.61 m x 0.61 m (2 ft x 2 ft) sampling squares and averaged over 20 s. No-fire and 600 kW fire results for water flux distributions are compared.

Considering the case of the horizontal ceiling, when no fire is present, we can observe from Figure 4-2(a) that the spray from the sprinkler falls evenly around the central location, with mass flux ~1.0 kg/m^2-s present in the region. Lower fluxes of the order of 0.5 kg/m^2-s are observed above and below the central region. Even lower fluxes are present on the left and right side. This is because the sprinkler arm was oriented in the x-direction.

Similar to the no fire case, when the 600 kW fire is present, the water mass flux distribution looks almost identical in the central region, see Figure 4-2(b). The 600 kW plume strength, being rather weak in comparison to the downward spray momentum originating from the K200 (K14) sprinkler operating at 3.4 bar (50 psi) with a 379 L/min (100 gpm) flow rate, does not cause a reduction in the mass flux distribution. Two differences though are apparent: 1) the reduction of the mass flux away from the central region can be observed, especially just north and south of the CUP array footprint where mass flux values decrease from ~0.37 kg/m^2-s to ~0.25 kg/m^2-s, and 2) a wider water flux distribution region can be observed when the fire is present.

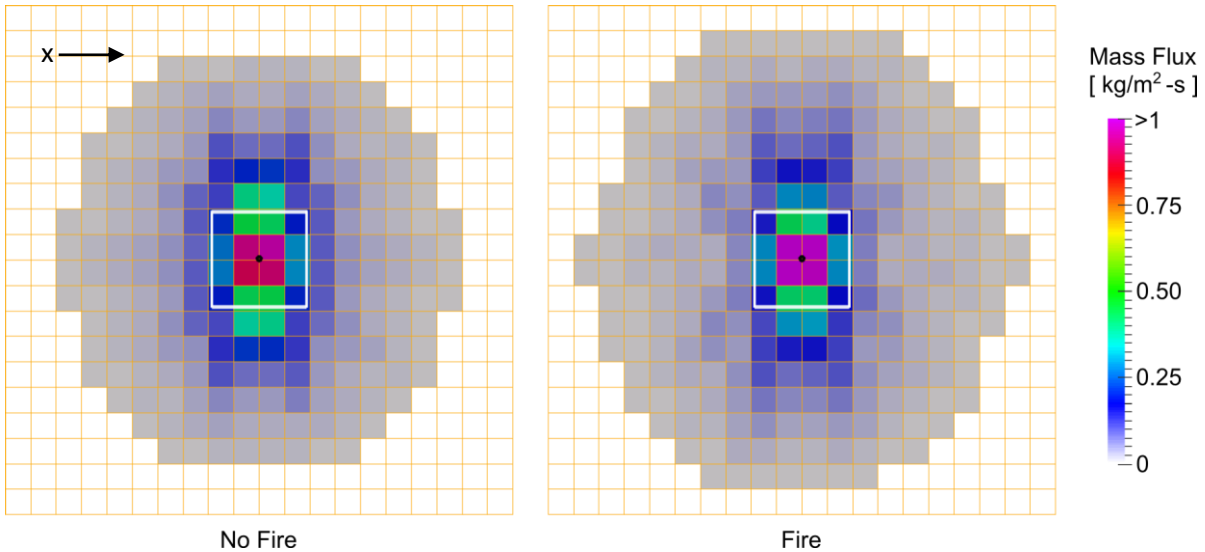

Figure 4-2: Droplet mass flux distributions are shown for one sprinkler below a horizontal ceiling located 3.05 m (10 ft) above the CUP array. Mass flux is computed at sampling squares of 0.37 m^2 (4 ft^2) area located 0.3 m (1 ft) above the top of the CUP rack storage array. Comparisons of (a) no fire scenario is made with (b) when a fire of 600 kW convective HRR is present. The projected sprinkler location on the collection plane is shown by a black dot and the footprint of the storage array is shown by the white square.

In Figure 4-3(a), the water mass flux distribution is shown for a ceiling inclined at 18.4° and the sprinkler deflector parallel to the floor with no fire present. The distribution is similar to the one shown for the 0° case, except for an elongated section below the lower side of the ceiling. This is due to droplets rebounding back. When the fire plume is present, this elongated region has lower water mass flux due to the presence of the ceiling jet, as can be seen in Figure 4-3(b). The presence of the weak fire plume does not alter the central region water distribution and, similar to the 0° case, reduction of mass flux in the outer regions occurs. Since the differences between the mass flux distribution between the 0° and 18.4° cases are minor, especially in the region surrounding the ignition location (a 1.2 m x 1.2 m or 4 ft x 4 ft region), it can be said that an inclination of 18.4° would not reduce the suppression effectiveness of the central activated sprinkler.

The effect of deflector orientation for an 18.4° inclination case is shown in Figure 4-4. When the deflector is kept parallel to the ceiling, and no fire is present, the highest mass flux region moves towards the elevated side, which can be seen in Figure 4-4(a). In the 1.2 m x 1.2 m (4 ft x 4 ft) central region, mass flux values between 0.5 and 0.75 kg/m^2-s are observed, whereas in the case of the deflector parallel to the ceiling, the mass flux values in this region were ~1 kg/m^2-s. The fire plume inhibits and/or evaporates the droplets in the central 1.2 m x 1.2 m (4 ft x 4 ft) region, which is evident in Figure 4-4(b); the mass flux values reduce down to less than 0.2 kg/m^2-s. The fire plume also entrains the droplets and moves them further away from the central region, as can be seen by the low mass flux values on the lower side of the ceiling as well as on the elevated side where the distribution is comparatively wider. Thus, suppression effectiveness in the event of activation of a single sprinkler will be reduced for the parallel-to-ceiling orientation.

The water distribution pattern shown in Figure 4-5(a) is for a 33.7° inclination, no fire, and parallel-to-floor orientation case. Similar water flux patterns are obtained compared to the 18.4° case. More droplets impinge on the lower side of the ceiling compared to the 18.4° case. However, the distribution region in the 33.7° case is more compact with higher mass flux values observed outside the central region: mass fluxes of >0.3 kg/m^2-s are present up to a distance of 2.4 m (8 ft) from the center. In the presence of the 600 kW fire plume, significant reduction in mass flux values is not observed and the overall distribution remains almost identical, see Figure 4-5(b).

For 33.7°, the parallel-to-ceiling orientation skews the water distribution towards the elevated side of the ceiling, see Figure 4-6(a). In the presence of the fire, the mass flux above the CUP array is drastically reduced and maximum values of <0.3 kg/m^2-s are seen in Figure 4-6(b). Clearly, compared to the case of the 33.7° slope with deflector parallel to the ceiling, this configuration would show the least suppression effectiveness.

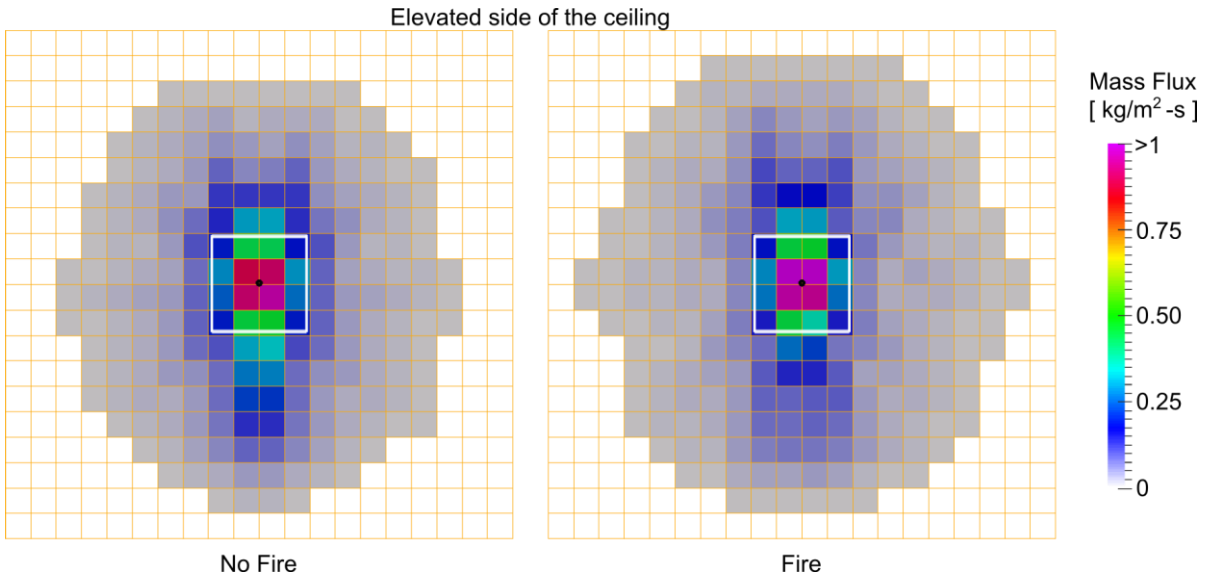

Figure 4-3: Droplet mass flux distributions are shown for one sprinkler below a ceiling inclined at 18.4°. Comparisons of (a) no fire scenario is made with (b) when a fire of 600 kW convective HRR is present. Sprinkler deflector is parallel to the floor.

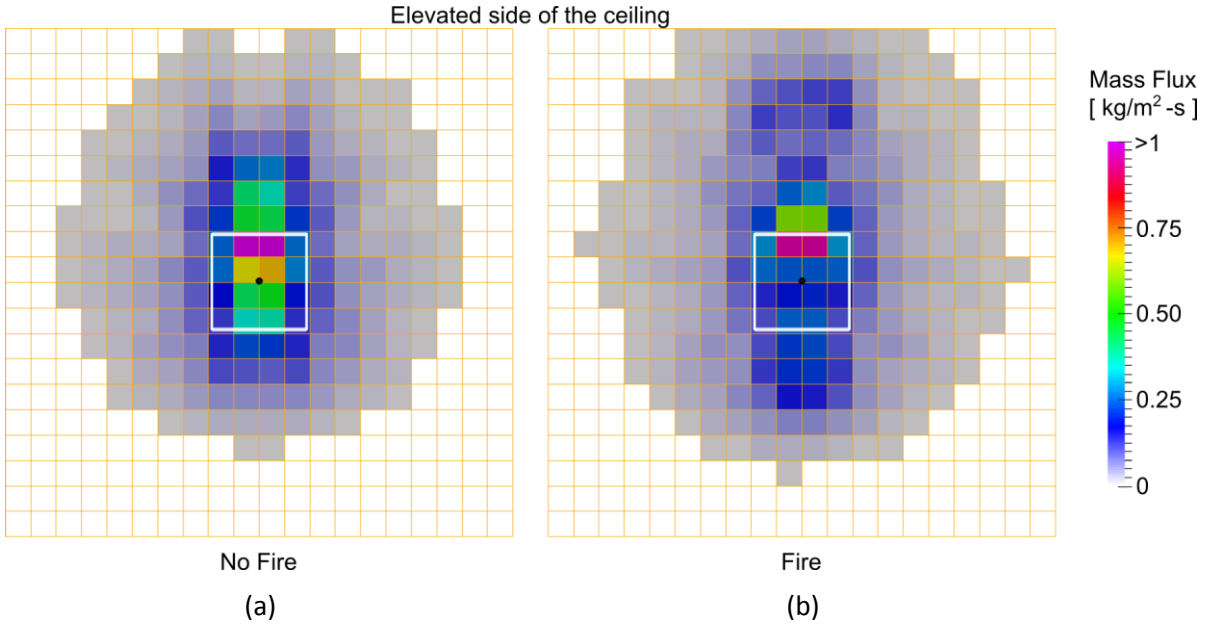

Figure 4-4: Droplet mass flux distributions are shown for one sprinkler below a ceiling inclined at 18.4°. Comparisons of (a) no fire scenario is made with (b) when a fire of 600 kW convective HRR is present. Sprinkler deflector is parallel to the ceiling.

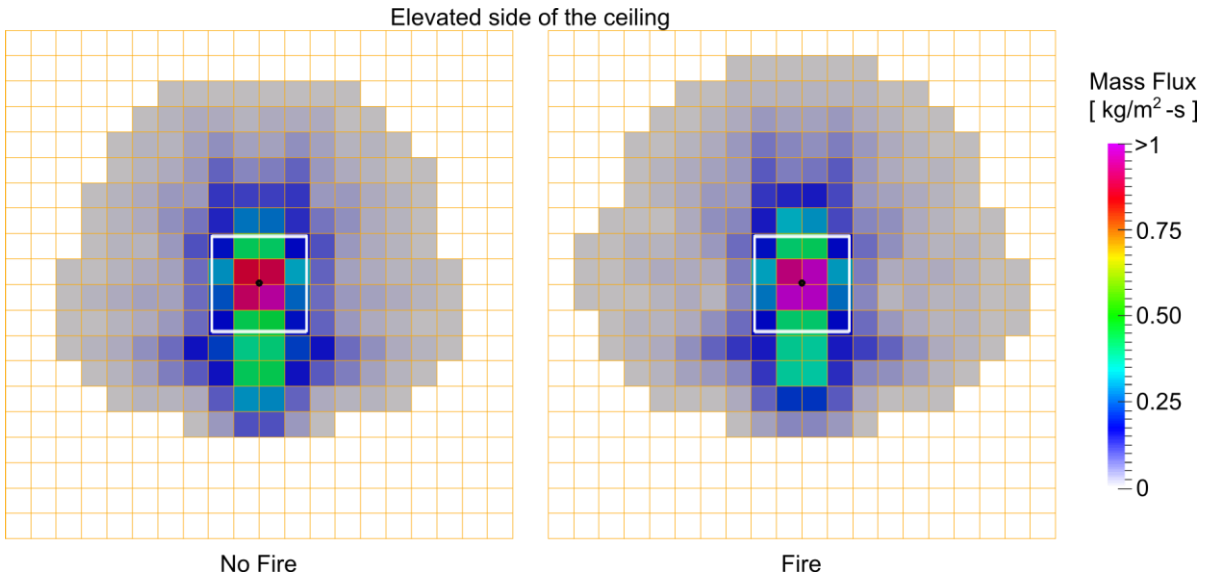

Figure 4-5: Droplet mass flux distributions are shown for one sprinkler below a ceiling inclined at 33.7°. Comparisons of (a) no fire scenario is made with (b) when a fire of 600 kW convective HRR is present. Sprinkler deflector is parallel to the floor.

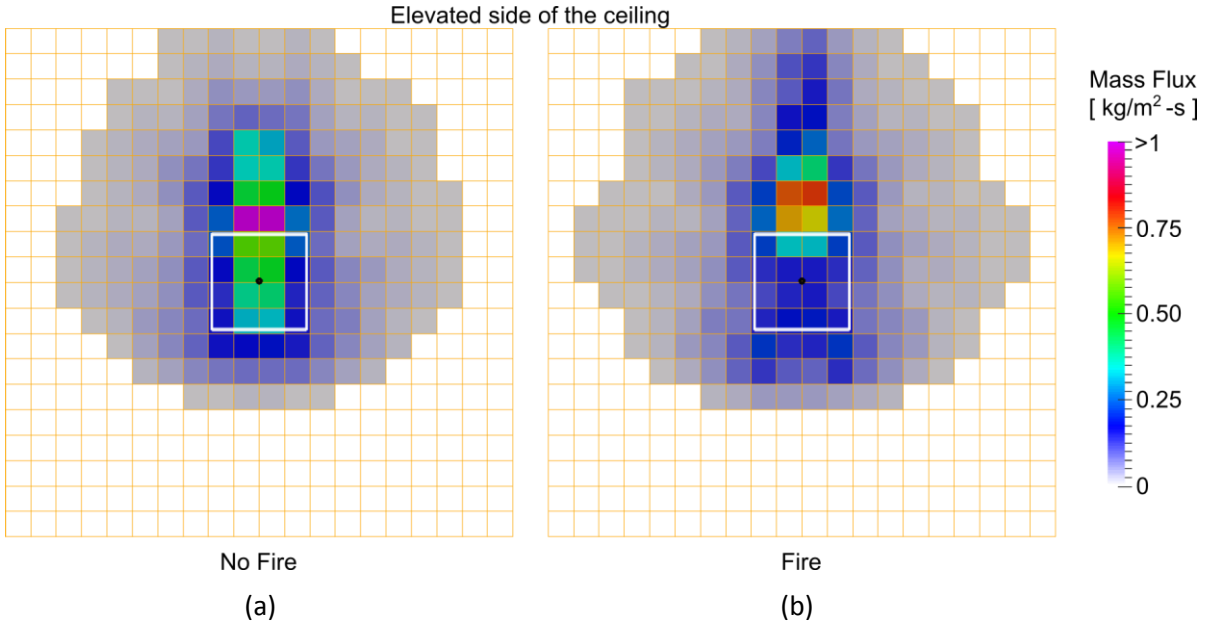

Figure 4-6: Droplet mass flux distributions are shown for one sprinkler below a ceiling inclined at 33.7°. Comparisons of (a) no fire scenario is made with (b) when a fire of 600 kW convective HRR is present. Sprinkler deflector is parallel to the ceiling.

In summary, from previous results, it can be said that the deflector orientation provides a greater variability in the mass flux results as compared to the ceiling inclination. With increasing ceiling inclination, some of the water hits the lower side of the ceiling when the deflector is parallel to the floor; however, the distribution over the CUP array does not get affected to a great extent. Detailed modeling of the aftermath of the spray impinging on the ceiling may be necessary while considering higher ceiling inclinations (e.g. 33.7°), when a water film may form below the ceiling resulting in flow downwards and away from the burning commodities.

To provide a clearer picture of the effect of ceiling inclination and deflector orientation, integrated mass flow rates through a 3.05 m x 3.05 m (10 ft x 10 ft) area above the CUP array are considered. In Figure 4-7(a), a comparison is made when no fire is present: the mass flow rate as a function of ceiling inclination is shown. The total collected mass flow rate when no fire is present does not change with inclination when the deflector is parallel to the floor; however, the same is not true when the deflector orientation is changed. The mass flow rate shows a slight reduction for the 18.4° ceiling, but a 19% reduction (from 3.2 kg/s for deflector parallel to the floor to 2.6 kg/s) can be seen for the 33.7° ceiling case. The differences become larger when the 600 kW fire is present, see Figure 4-7(b). A mass flow rate decline of 25% for the 18.4° case and an even greater reduction of 49% for the 33.7° case occurs.

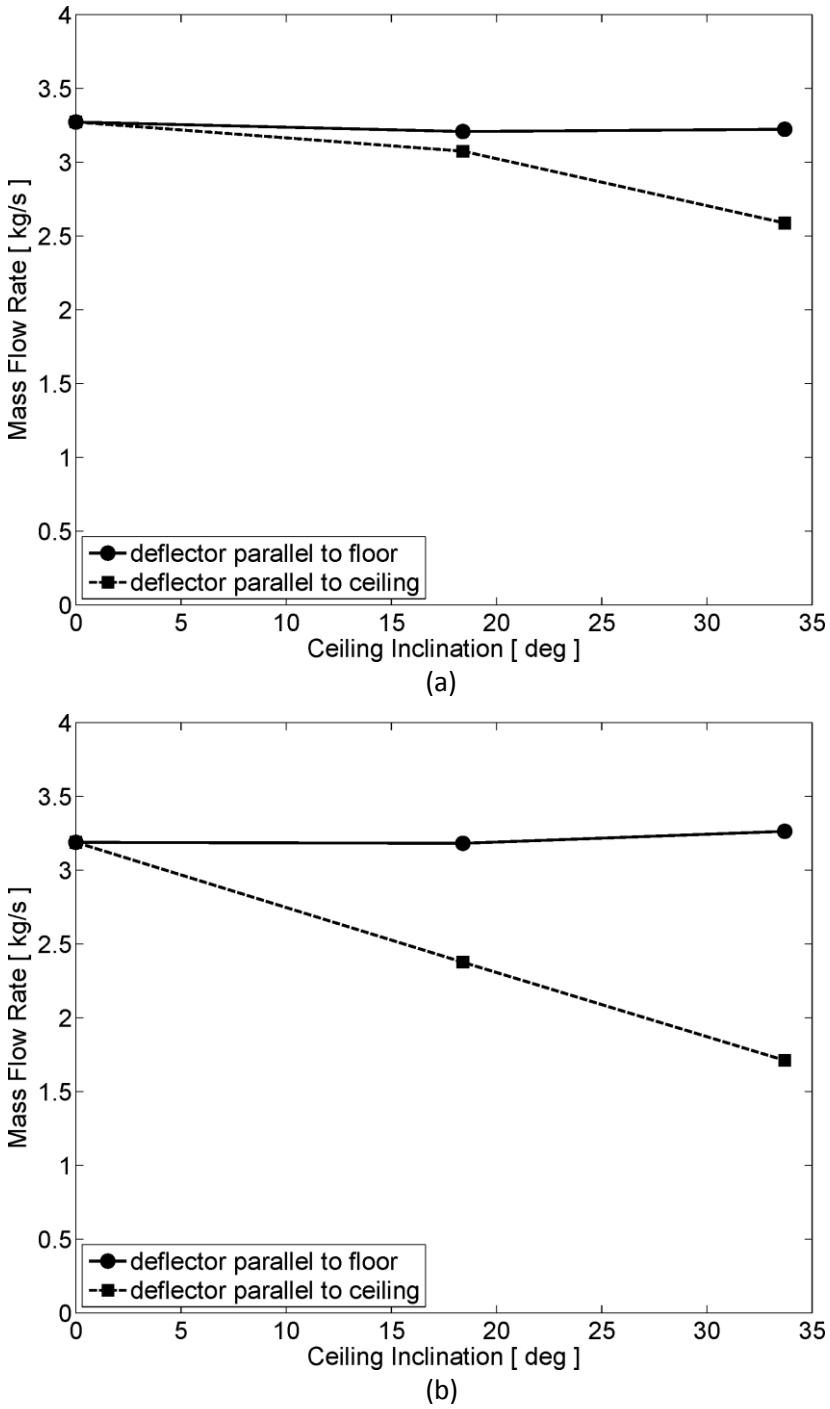

Figure 4-7: Droplet mass flow rate through a 3.05 m x 3.05 m (10 ft x 10 ft) sampling area surrounding the ignition location at a height of 0.3 m (1 ft) above the CUP rack-storage array as a function of ceiling inclination. Single K200 (K14) sprinkler located above the ignition location: (a) without fire, and (b) with a fire of constant 600 kW convective HRR.

4.4 Water Flux Distributions from Four Sprinklers

The impact of ceiling inclination and deflector orientation was studied for the scenario when the fire is located among four sprinklers. In this case, the vertical distance of the sprinkler deflector varies when the ceilings are inclined. The two sprinklers on the elevated side are at higher height compared to the two located on the lower side of the ceiling. This elevation difference increases with increasing ceiling inclination angle.

In Figure 4-8, instantaneous snapshots of sprays originating from the sprinklers are shown for the three inclination angles (0°, 18.4° and 33.7°) and two orientations of the deflector (parallel to the floor or to the ceiling). When the ceiling is horizontal, the droplets are confined around the central region where the fire is present, see Figure 4-8(a). Inclining the ceiling at 18.4°, with the deflectors parallel to the floor, two sprinklers are now located higher and the spray pattern changes with higher mass flux expected below the lower sprinklers, see Figure 4-8(b). Keeping the inclination at 18.4° and making the deflector parallel to the ceiling, the higher located sprinklers provide a majority of the droplets away from the fire location. However, as can be observed in Figure 4-8(c), the lower sprinklers in this case provide more water directed at the central fire location as compared to when the deflectors are parallel to the floor.

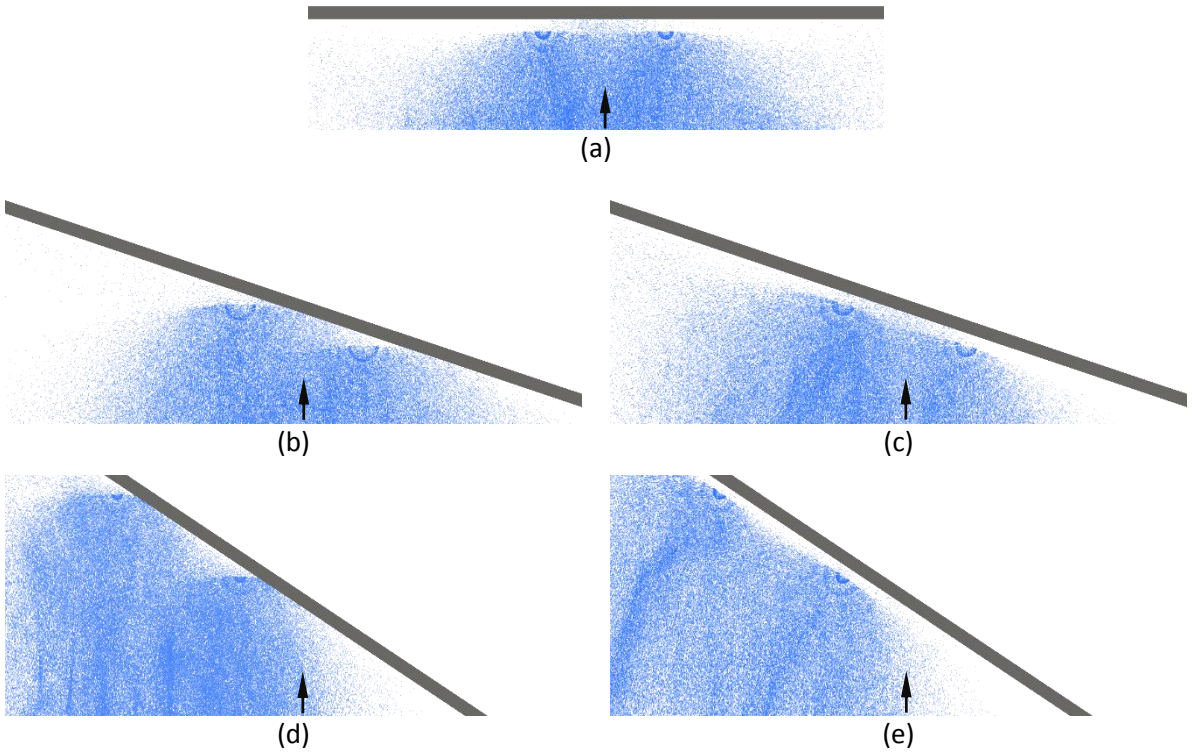

Figure 4-8: Instantaneous snapshots of sprays originating from four K200 (K14) sprinklers (two injection regions visible in the images) for (a) 0°, deflector parallel to floor, (b) 18.4°, deflector parallel to floor, (c) 18.4°, deflector parallel to ceiling, (d) 33.7°, deflector parallel to floor, and (e) 33.7°, deflector parallel to ceiling. A fire plume of 2.6 MW convective HRR was present. Plume centerline is shown by the vertical arrows.

For the 33.7° inclination cases, the four sprinklers to activate are located in the elevated side of the ceiling. Therefore, irrespective of the deflector orientation, the majority of the droplets are not directed towards the central fire region. In Figure 4-8(d) sprays with deflectors parallel to the floor, are shown, with the majority of the water mass not directed towards the fire. In comparison, when the deflectors are parallel to the ceiling, even less water is incident on to the fire region, as shown in Figure 4-8(e).

Droplet mass flux distributions are next presented for four sprinklers. As described earlier, the droplet mass is averaged over 20 s intervals at 0.6 m x 0.6 m (2 ft x 2 ft) square sampling areas located on the collection plane 0.3 m (1 ft) above the CUP array.

For the 0° inclination case, with the fire convective HRR held constant at 2.6 MW, the maximum mass flux occurs right below the locations of the sprinklers. Symmetric patterns of mass flux distributions are observed to occur around the sprinkler locations, with higher mass flux values above and below compared to the lateral values, as seen in Figure 4-9. Due to the presence of the 2.6 MW fire plume, the mass flux values in the central 1.2 m x 1.2 m (4 ft x 4 ft) area are small (<0.3 kg/m^2-s). In comparison, the peak mass flux values below the sprinklers is ~2 kg/m^2-s.

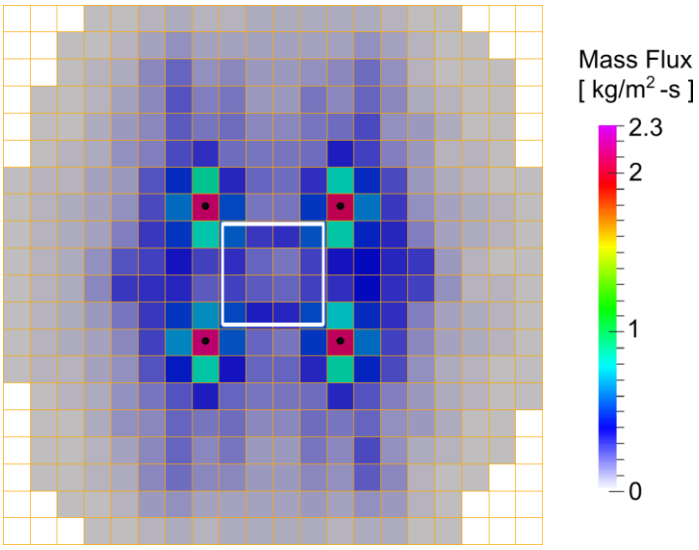

Figure 4-9: Droplet mass flux distribution is shown for four sprinklers below a horizontal ceiling located 3.05 m (10 ft) above the CUP array. Mass flux is computed at sampling squares of 0.37 m^2 (4 ft^2) area located 0.3 m (1 ft) above the top of the CUP rack storage array. A fire with a constant 2.6 MW convective HRR is present. Projected sprinkler locations on the collection plane are indicated by black dots and the footprint of the CUP array is shown by the white square. Sprinkler deflectors are parallel to the floor.

When the ceiling inclination is 18.4° and the sprinkler deflectors are parallel to the floor, the mass flux below the sprinklers on the lower side of the ceiling is ~2.3 kg/m^2-s, compared to the mass flux below the sprinklers on the elevated side (<2 kg/m^2-s). The water distribution is skewed towards the elevated side as well, as seen in Figure 4-10, with the central region above the ignition location showing relatively low

mass flux due to the presence of the plume in this region. The droplets that impinge the lower side of the ceiling are carried away or get evaporated due to the presence of the stronger ceiling jet flow and higher temperatures compared to the single sprinkler case. The distribution pattern for the 18.4° ceiling with deflectors parallel to the floor is quite similar to the one for the case with a 0° inclination shown in Figure 4-9. This indicates that a ceiling inclination of 18.4° may be considered similar to a ceiling with a 0° inclination for sprinkler protection recommendation purposes.

For deflectors parallel to the ceiling and the ceiling inclination of 18.4°, the water flux distribution above the rack-storage array is shown in Figure 4-11. Compared to the distribution for deflectors parallel to the floor shown in Figure 4-10, somewhat higher mass flux is distributed around each sprinkler locations. However, the maximum mass flux regions show a shift towards the elevated side. The maximum values are, however, comparable to the case with deflectors parallel to the floor. Essentially, no major differences can be easily discerned between the deflector orientations when the mass flux distributions are compared. This is in contrast to the single sprinkler configuration for which there was a 19% reduction in integrated mass flux in the case of deflector parallel to the ceiling.

In the case of the ceiling inclined at 33.7°, the four sprinklers are all located on the elevated side of the ceiling. The greater distance between the fire and the sprinkler locations, especially for the ones higher up in elevation, reduces the effectiveness of sprinkler sprays to provide adequate water flux for control of fire growth or pre-wetting of neighboring commodities. As shown in Figure 4-12, when the deflectors are parallel to the floor, some amount of water is deposited near the fire region by the two sprinklers closest to the ignition location.

The configuration of deflectors parallel to the ceiling, for ceilings inclined at 33.7°, provides an even lower distribution of water mass flux in the pre-wetting region, as shown in Figure 4-13. The higher values of mass flux at distances >3.05 m (10 ft) are contributed by the sprinklers closest to the CUP rack-storage array. This area is quite far away from where pre-wetting is required. The contribution from the higher sprinklers are not shown as most of the water mass flux lands beyond 6.1 m (20 ft) where data was not recorded. Quite clearly, the 33.7° ceiling inclination will not be conducive towards sprinkler protection designs, due both to the sprinkler activation patterns and ineffectiveness of the sprinkler sprays to provide water flux in the fire growth region.

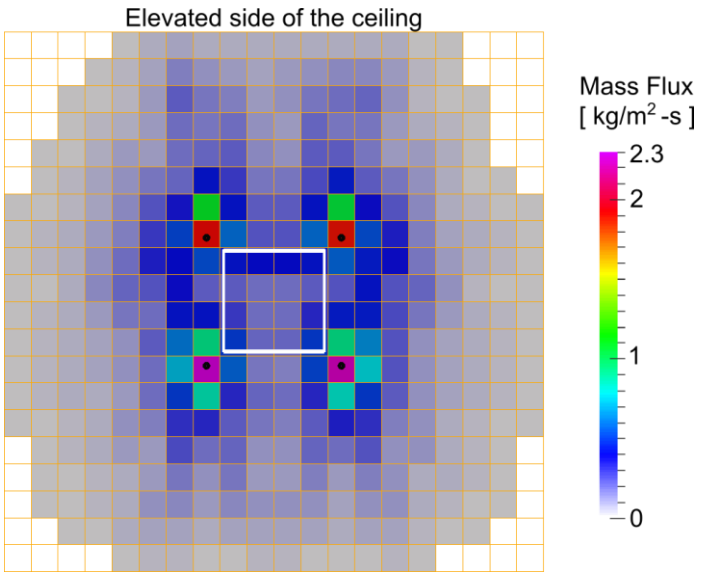

Figure 4-10: Droplet mass flux distributions are shown for four sprinklers below a ceiling inclined at 18.4°. A fire with a constant 2.6 MW convective HRR is present. Sprinkler deflectors are parallel to the floor.

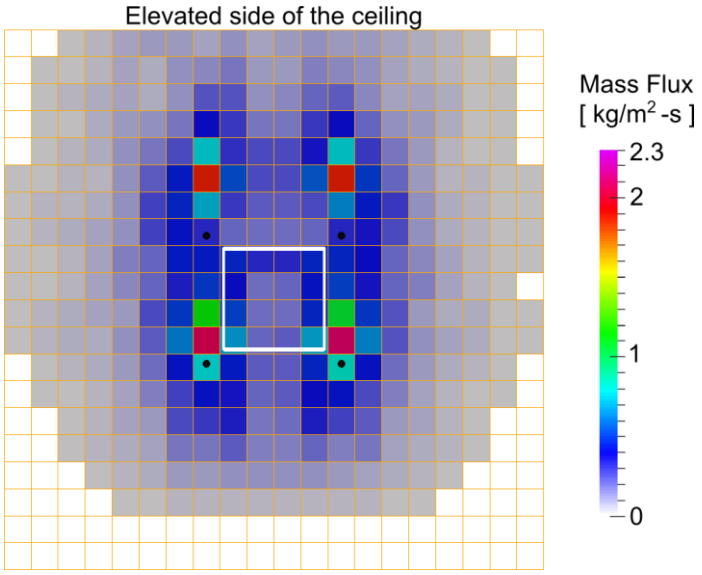

Figure 4-11: Droplet mass flux distributions are shown for four sprinklers below a ceiling inclined at 18.4°. A fire with a constant 2.6 MW convective HRR is present. Sprinkler deflectors are parallel to the ceiling.

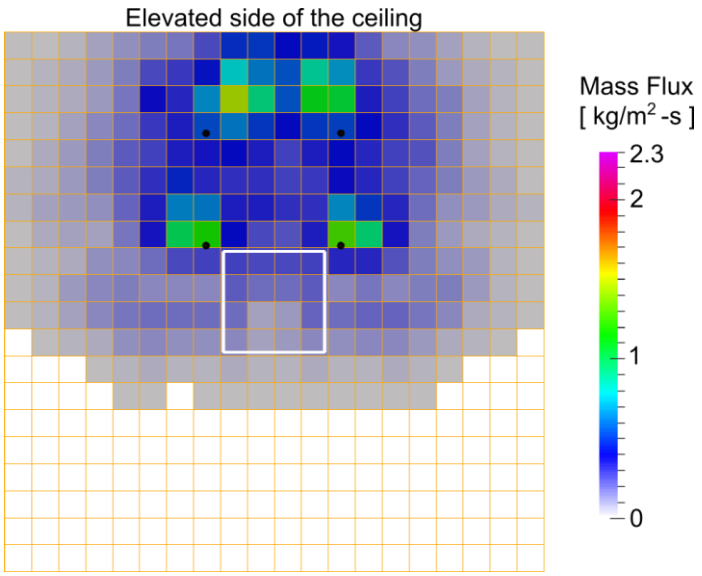

Figure 4-12: Droplet mass flux distributions are shown for four sprinklers below a ceiling inclined at 33.7°. A fire with a constant 2.6 MW convective HRR is present. Sprinkler deflectors are parallel to the floor.

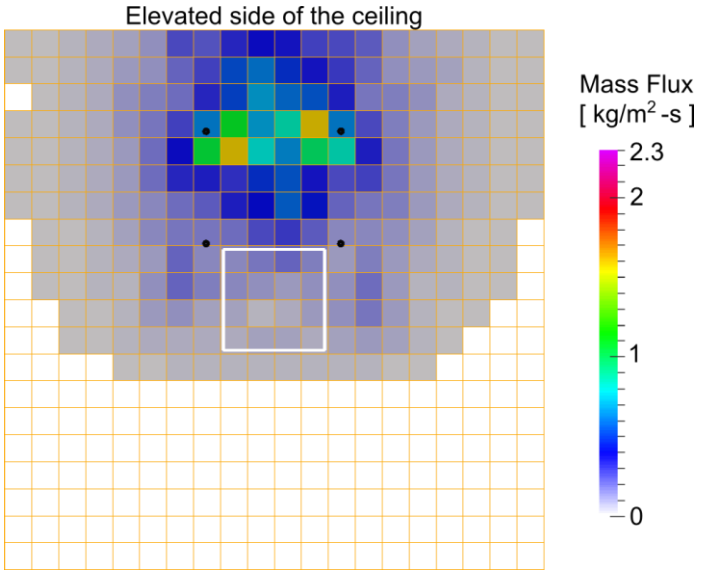

Figure 4-13: Droplet mass flux distributions are shown for four sprinklers below a ceiling inclined at 33.7°. A fire with a constant 2.6 MW convective HRR is present. Sprinkler deflectors are parallel to the ceiling.

In summary, compared to the single sprinkler scenario described earlier, the four-sprinkler cases show that the deflector orientation is not the primary variable affecting the effectiveness of sprinkler sprays. On the contrary, the ceiling inclination has a stronger influence on the water distribution patterns. However, significant differences in water mass flux distributions were not noticeable between the 0° and 18.4° inclination cases. The major differentiator, in terms of water distribution, was the location of first four sprinkler activations for the 33.7° inclination case. When the ceiling inclination is 33.7°, the water flux provided by the sprinkler sprays may be ineffective in controlling fire spread.

The effect of ceiling inclination on water mass flux distribution can be summarized by comparing the total mass flow rate through a 3.05 m x 3.05 m (10 ft x 10 ft) area above the CUP array. Figure 4-14 shows such a comparison when the 2.6 MW fire is present. The mass flow rates when the ceiling is inclined at 18.4° are almost equal to when the ceiling was horizontal, irrespective of the orientation of the deflectors. The average mass flow rate decrease from the 0° case (4.1 kg/s) to the 33.7° case is significant, especially when the deflector is parallel to the ceiling (1 kg/s, a decrease of 76%) as compared to when the deflector is parallel to the floor (1.9 kg/s, a decrease of 54%).

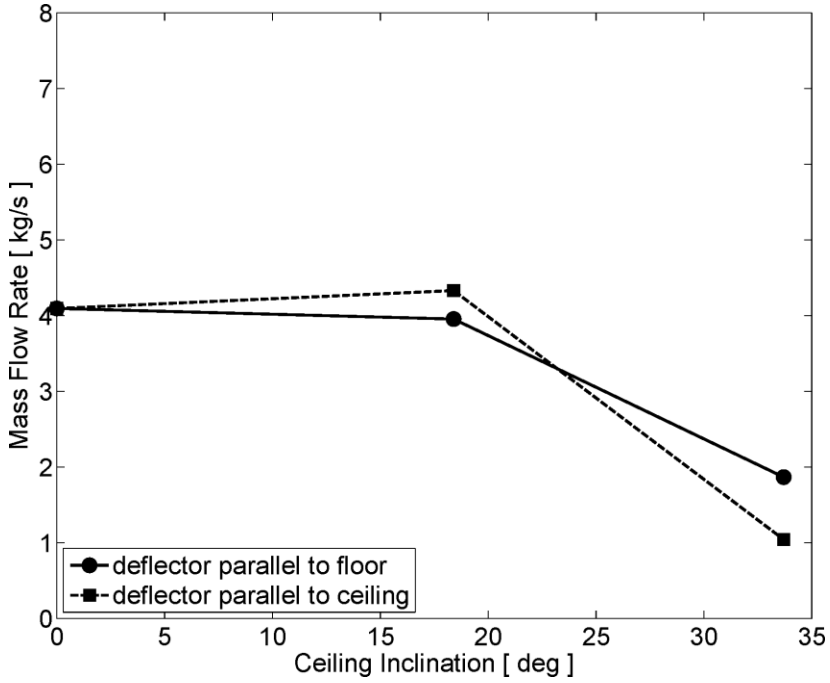

Figure 4-14: Time-averaged droplet mass flow rate through a 3.05 m x 3.05 m (10 ft x 10 ft) sampling area surrounding the ignition location at a height of 0.3 m (1 ft) above the CUP rack-storage array as a function of ceiling inclination. Four K200 (K14) sprinklers located below the ceilings with a fire source of constant 2.6 MW convective HRR.

4.5 Summary

When the sprinkler is located directly above the fire plume, the deflector orientation strongly affects the water flux that can reach the fire source and the pre-wetting region. As the slope is increased, the parallel-to-the-floor orientation can maintain a fairly consistent water flux to the fire region. In the absence of a fire plume, the parallel-to-the-ceiling orientation also maintains a consistent water flux even at 18.4°, but deviates strongly from the parallel-to-the-floor orientation at the 33.7° inclination with a 19% reduction in water flow.

In the presence of a fire plume (600 kW convective HRR), this effect is exacerbated. The parallel-to-floor results show little deviation from the spray-only scenario and are constant with inclination angle. The parallel-to-ceiling orientation, however, shows a significant reduction in water flux at the 18.4° slope (25%) and an even greater reduction at 33.7° (49%).

For a fire plume among four sprinklers, the 33.7° inclination adversely impacts the spray density on the fire because of a highly skewed activation pattern. This results in the first four sprinkler activations occurring on the elevated side. The water flux to the fire region is reduced by 54-76% when compared to the horizontal case. For ceiling slopes 18.4° and below, the water flux on the 3.05 m x 3.05 m (10 ft x 10 ft) area is less sensitive to sprinkler orientation than for the case of a single sprinkler centered over the fire plume. This is because the activations on the lower side for the parallel-to-ceiling case actually result in water being directly projected onto the fire region. This observation is based on the assumption that four sprinklers surrounding the fire source activate simultaneously, and only the water flux on top of the fire source (3.05 m x 3.05 m area) are evaluated.

5. Conclusions and Recommendations

In the present study, FireFOAM was first validated for ceiling jet flows below inclined ceilings. Predicted temperature and velocity showed good agreement with experimental data. Simulations were then conducted for determining sprinkler activation patterns and times for a range of ceiling slopes/inclinations. A growing fire on a 2 x 2 x 3 CUP rack-storage array with a maximum convective HRR of 15 MW was used as the plume source. Developing ceiling jet flow patterns were presented using temperature contours. Sprinkler activation calculations were made by decoupling activation from other suppression phenomena. Activation times and patterns below the inclined ceilings were compared against horizontal ceiling results. A ceiling clearance of 3.05 m (10 ft) to the midpoint of the ceiling was considered in the study. The effect of increasing the ceiling clearance to 6.1 m (20 ft) was also investigated. Comparison was also made between quick-response, ordinary temperature (QR/OT) and standard-response, high temperature (SR/HT) sprinklers.

In addition, sprinkler spray simulations were conducted by selecting fixed fire source sizes for two scenarios: 1) when one sprinkler above the ignition location activates, and 2) when four sprinklers operate. In the case of four sprinklers, an average HRR was selected based on the sprinkler locations and predicted activation times. Water mass flux distributions were compared for various ceiling inclinations and sprinkler deflector orientations.

Based on the range of conditions explored, the following conclusions can be drawn:

- Results from activation simulations involving QR/OT sprinklers show that ceilings up to and including 18.4° inclination have similar activation times and patterns as horizontal ceiling for the four sprinklers immediately adjacent to the fire source.
- Increasing the inclination to 26.6° produces significant delays in activations on the lower side of the ceiling. The number of sprinklers activated on the elevated side also greatly exceeds the number of activations on the lower side when the ceiling inclination is ≥26.6°.
- For SR/HT sprinklers, the average delay time for activations of the four sprinklers surrounding the ignition location increases for the 18.4° inclination case. Four more activations take place in the elevated section before the sprinklers below the lower side activate, indicating the activation pattern skewness is accentuated with the use of these sprinklers. It is also to be noted that, compared to the QR/OT sprinklers, these sprinklers provide greater activation delays on average.
- Based on the two clearances included in the activation simulations for the 18.4° inclined ceiling (3.05 m and 6.1 m or 10 ft and 20 ft), it was found that increasing the ceiling clearance to 6.1 m (20 ft), the average activation time for the four sprinklers surrounding the ignition location increased by ~3 s and ~5 s for QR/OT and SR/HT sprinklers, respectively. Such activation time delays may have an adverse impact on protection design. For spray calculations involving a single sprinkler located directly above the ignition location, it was found that the deflector orientation strongly affects the water flux that reaches the fire source and the pre-wetting region. As the ceiling inclination increases, the water flux on top of the commodity was found to reduce when

the sprinkler deflector was kept parallel to the ceiling. This reduction of water flux was significantly greater when a 600 kW fire plume was present (25% for the 18.4° and 49% for the 33.7° ceilings). On the other hand, as the inclination was increased, the parallel-to-the-floor orientation could maintain a fairly constant water flux to the fire region.

- For a fire plume among four sprinklers, it was determined that the ceiling slope at 33.7° adversely impacts the spray density on the fire because of a highly skewed activation pattern, which results in the first four sprinkler activations occurring below the elevated side of the ceiling. For the 33.7° case, the water flux to the fire region is reduced by 54-76% as compared to the horizontal ceiling case.
- For ceiling slopes 18.4° and below, the sprinkler orientation for the fire plume among four sprinklers case is less important than for the case of a single sprinkler centered over the fire plume. This is because the activations downward from the centerline for the parallel-to-ceiling case actually result in water being projected towards the fire region. This observation is based on the assumption that four sprinklers surrounding the fire source activate simultaneously, and only the water flux on top of the fire source (3.05 m x 3.05 m area) are evaluated.
- Considering the significant effect of the deflector orientation on the water flux for a sprinkler above the ignition location and the relatively reduced effect of the orientation for the among four sprinklers case, the orientation parallel to the floor is preferable for a variety of fire scenarios among the cases studied.

Further evaluations of the conclusions should be made by conducting large-scale fire tests and/or by conducting numerical simulations. Several aspects have been neglected while conducting this study as the goal was to capture the first order physical effects on sprinkler activations and spray patterns. Some of these aspects are the presence of end-walls in buildings, obstructions to the ceiling flows caused by purlins and girders, inclusion of suppression phenomena in the modeling, etc. Before making general recommendations towards sprinkler protection schemes, it would be prudent to consider the effects of these aspects.

References

1. Custom Spray Solutions, Inc. [Online]. http://www.customspraysolutions.com

2. FireFOAM. [Online]. http://www.fmglobal.com/modeling

3. Y. Wang, P. Chatterjee, and J. L. de Ris, "Large Eddy Simulation of Fire Plumes," *Proceedings of the Combustion Institute*, vol. 33, no. 2, pp. 2473-2480, 2011.

4. K. E. Isman, "Challenges for the Fire Sprinkler Industry," *Fire Protection Technology*, May 9, 2012.

5. R. L. Vettori, "Effect of Beamed, Sloped, and Sloped Beamed Ceilings on the Activation Time of a Residential Sprinkler," *NIST Report NISTIR 7079*, December 2003.

6. H.-C. Kung, R. D. Spaulding, and P. Stavrianidis, "Fire Induced Flow under a Sloped Ceiling," *Fire Safety Science*, vol. 3, pp. 271-280, 1991.

7. J. Floyd, E. Budnick, M. Boosinger, J. Dinaburg, and H. Boehmer, "Analysis of the Performance of Residential Sprinkler Systems with Sloped or Sloped and Beamed Ceilings," *Fire Protection Research Foundation Report*, July 2010.

8. R. G. Bill Jr. and E. E. Hill Jr., "Sprinkler Protection of Manufactured Homes with Sloped Ceilings Using Prototype Limited Water Supply Sprinklers," *Fire Technology*, vol. 31, no. 1, pp. 5-16, 1995.

9. W. D. Davis, G. P. Forney, and R. W. Bukowski, "Field Modeling: Simulating the Effect of Sloped Beamed Ceilings on Detector and Sprinkler Response," *NIST Technical Report, Year 2*, October 1994.

10. Fire Dynamics Simulator (FDS). [Online]. http://code.google.com/p/fds-smv

11. J. Floyd, S. Riahi, C. Mealy, and D. Gottuk, "Smoke Detector Spacing Requirements Complex Beamed Sloped Ceilings – Volume 2: Modeling of and Requirements for Parallel Beamed, Flat Ceiling Corridors and Beamed, Sloped Ceilings," *Fire Protection Research Foundation Report*, April 2008.

12. E. Carlsson, "Comparison of Sprinkler Activation in Flat and Sloping Ceilings using FDS 6," Lund University, Report 5404, 2013.

13. "FM Global Data Sheet 8-9, Storage of Class 1, 2, 3, 4 and Plastic Commodities," FM Global, Norwood, MA, July 2011.

14. "FM Global Data Sheet 2-0, Installation Guidelines for Automatic Sprinklers," FM Global, Norwood, MA, January 2014.

15. "NFPA 13, Standard for Installation of Sprinkler Systems," National Fire Protection Association, Quincy, MA, 2013.

16. Custom Spray Solutions (CSS), "Analysis of Sloped Ceiling and Sprinkler Orientation Impact on Delivered Density," unpublished, February 2013.

17. X. Zhou, S. P. D'Aniello, and H.-Z. Yu, "Spray Characterization Measurements of a Pendent Fire Sprinkler," *Fire Safety Journal*, vol. 54, pp. 36-48, 2012.

18. "OpenFOAM: The Open Source CFD Toolbox, User Guide, Version 2.2.0," February 22, 2013.

19. OpenFOAM User Guide: 5.4 Mesh generation with snappyHexMesh. [Online]. http://cfd.direct/openfoam/user-guide/snappyhexmesh

20. P. Chatterjee, J. L. de Ris, Y. Wang, and S. B. Dorofeev, "A Model for Soot Radiation in Buoyant Diffusion Flames," *Proceedings of the Combustion Institute*, vol. 33, no. 2, pp. 2665–2671, 2011.

21. P. Chatterjee, Y. Wang, K. V. Meredith, and S. B. Dorofeev, "Application of a Subgrid Soot-radiation Model in the Numerical Simulation of a Heptane Pool Fire," *Proceedings of the Combustion Institute*, vol. 35, no. 3, pp. 2573-2580, 2015.

22. M. Chaos, M. M. Khan, N. Krishnamoorthy, and S. B. Dorofeev, "Evaluation of Optimization Schemes and Determination of Solid Fuel Properties for CFD Fire Models Using Bench-scale Pyrolysis Tests," *Proceedings of the Combustion Institute*, vol. 33, no. 2, pp. 2599-2606, 2011.

23. M. Chaos, M. M. Khan, and S. B. Dorofeev, "Pyrolysis of Corrugated Cardboard in Inert and Oxidative Environments," *Proceedings of the Combustion Institute*, vol. 34, no. 2, pp. 2583–2590, 2012.

24. N. Ren, Y. Wang, and A. Trouve, "Large Eddy Simulation of Vertical Turbulent Wall Fires," *Procedia Engineering*, vol. 62, pp. 443-452, 2013.

25. P. Chatterjee, K. V. Meredith, B. Ditch, H.-Z. Yu, Y. Wang, and F. Tamanini, "Numerical Simulations of Strong-Plume Driven Ceiling Flows," *Fire Safety Science*, vol. 11, pp. 458-471, 2014.

26. K. V. Meredith, Y. Xin, and J. de Vries, "A Numerical Model for Simulation of Thin-film Water Transport over Solid Fuel Surfaces," *Fire Safety Science*, vol. 10, pp. 415-428, 2011.

27. K. V. Meredith, J. de Vries, Y. Wang, and Y. Xin, "A Comprehensive Model for Simulating the Interaction of Water with Solid Surfaces in Fire Suppression Environments," *Proceedings of the Combustion Institute*, vol. 34, no. 2, pp. 2719–2726, 2012.

28. Y. Wang, K. V. Meredith, X. Zhou, P. Chatterjee, Y. Xin, M. Chaos, N. Ren, and S. B. Dorofeev, "Numerical Simulation of Sprinkler Suppression of Rack Storage Fires," *Fire Safety Science*, vol. 11, pp. 1170-1183, 2014.

29. K. V. Meredith, P. Chatterjee, X. Zhou, Y. Wang, and H.-Z. Yu, "Validation of Spray Water Distribution Patterns for the K11.2 Sprinkler in the Presence of a Rack Storage Fire Plume Generator," *Proceedings of the 13th Fire Science and Engineering Conference (INTERFLAM)*, pp. 307-316, 2013.

30. K. V. Meredith, P. Chatterjee, Y. Wang, and Y. Xin, "Simulating Sprinkler Based Rack Storage Fire Suppression under Uniform Water Distribution," *Proceedings of the Seventh International Seminar on Fire & Explosion Hazards*, pp. 511-520, 2013.

31. G. Agarwal, A. Gupta, M. Chaos, K. V. Meredith, and Y. Wang, "An Experimental and Modeling Approach to Investigate the Burning Behavior of Cartoned Unexpanded Plastic Commodity," in *9th U.S. National Combustion Meeting*, Cincinnati, OH, 2015.

32. A. Gupta, K. V. Meredith, G. Agarwal, S. Thumuluru, Y. Xin, M. Chaos, and Y. Wang, "Development of a CFD Model for Large-Scale Rack-Storage Fires of Cartoned Unexpanded Plastic Commodity," in *2nd European Symposium of Fire Safety Science*, Nicosia, Cyprus, 2015.

fmglobal.com/researchreports

In the United Kingdom:
FM Insurance Company Limited
1 Windsor Dials, Windsor, Berkshire, SL4 1RS
Regulated by the Financial Services Authority